Annual Review of Astronomy and Astrophysics

Magnetars

Victoria M. Kaspi[1] and Andrei M. Beloborodov[2]

[1]Department of Physics and McGill Space Institute, McGill University, Montreal H3W 2C4, Canada; email: vkaspi@physics.mcgill.ca

[2]Physics Department and Columbia Astrophysics Laboratory, Columbia University, New York, NY 10027; email: amb@phys.columbia.edu

Annu. Rev. Astron. Astrophys. 2017. 55:261–301

First published as a Review in Advance on June 21, 2017

The *Annual Review of Astronomy and Astrophysics* is online at astro.annualreviews.org

https://doi.org/10.1146/annurev-astro-081915-023329

Keywords

neutron stars, magnetic fields, radio pulsars, flares, X-ray astronomy, X-ray outbursts

Abstract

Magnetars are young and highly magnetized neutron stars that display a wide array of X-ray activity including short bursts, large outbursts, giant flares, and quasi-periodic oscillations, often coupled with interesting timing behavior including enhanced spin-down, glitches, and antiglitches. The bulk of this activity is explained by the evolution and decay of an ultrastrong magnetic field, stressing and breaking the neutron-star crust, which in turn drives twists of the external magnetosphere and powerful magnetospheric currents. The population of detected magnetars has grown to about 30 objects and shows unambiguous phenomenological connection with highly magnetized radio pulsars. Recent progress in magnetar theory includes explanation of the hard X-ray component in the magnetar spectrum and development of surface heating models, explaining the sources' remarkable radiative output.

Contents

1. INTRODUCTION AND HISTORICAL OVERVIEW 262
2. OVERVIEW OF THE KNOWN MAGNETAR POPULATION 264
2.1. Basic Properties 264
2.2. Spatial Distribution 265
2.3. Associations with Supernova Remnants and Wind Nebulae 265
2.4. Relationship to High-Magnetic-Field Radio Pulsars 268
3. TEMPORAL BEHAVIOR 269
3.1. X-ray Pulsations, Spin-Down, and Timing 269
3.2. Transient Radiative Behavior: Bursts, Outbursts, Giant Flares, and Quasi-Periodic Oscillations 272
3.3. Temporal Properties of Low-Frequency Emission 275
4. RADIATION SPECTRUM 277
4.1. Burst Spectra 277
4.2. Persistent Emission 278
4.3. X-ray Spectral Evolution in Outburst 280
4.4. Low-Frequency Emission 282
5. MECHANISM OF MAGNETAR ACTIVITY 282
5.1. Internal Dynamics 282
5.2. Internal Heating and Surface Emission 284
5.3. Flares 287
5.4. Gradual Energy Release in the Twisted Magnetosphere 290
5.5. Spin-Down Torque 293
6. CONCLUSIONS AND FUTURE WORK 294

1. INTRODUCTION AND HISTORICAL OVERVIEW

Magnetars are a class of young neutron stars that exhibit dramatic variability across the electromagnetic spectrum—particularly at X-ray and soft γ-ray energies—ranging from few-millisecond bursts to major month-long outbursts. Some magnetar outbursts include X-ray and soft γ-ray flares that briefly outshine the entire cosmic hard X-ray sky put together. Magnetar emission is powered by the decay of enormous internal magnetic fields, which is why Duncan & Thompson (1992) coined the name magnetar. The known magnetar population today consists of just 29 sources; however, they are likely to represent at least 10% of the young neutron-star population (and possibly a much larger fraction). There are nearly 1,000 papers on the subject, a testament to their relevance to many branches of astrophysics today, from gravitational waves to superluminous supernovae to gamma-ray bursts (GRBs) to fast radio bursts.

Several other magnetar reviews have been written, some primarily observational (Rea & Esposito 2011), some primarily theoretical (Turolla et al. 2015), and some, like this one, a combination (Woods & Thompson 2006, Mereghetti et al. 2015). For reviews putting magnetars into the context of the broader neutron-star population, see Kaspi (2010) and Kaspi & Kramer (2015).

Historically, magnetars first appeared in astronomy under the names soft gamma repeaters (SGRs) and anomalous X-ray pulsars (AXPs). The first published report of a magnetar detection was in 1979 when repeated bursts were seen by space-based hard X-ray/soft gamma-ray instruments aboard the interplanetary space probes Venera 11 and 12 (Mazets et al. 1979a,b; Mazets &

Golenetskii 1981). Although magnetars were first thought to have the same origin as the classical GRBs, repeated bursts, including one enormous flare on March 5, 1979, from the direction of the star-forming Dorado region in the Large Magellanic Cloud (LMC) (Mazets et al. 1979b), rendered this unlikely. The repeated bursts had decidedly softer spectra than those of the GRBs, hence the designation as SGRs. Additional soft GRBs from what is known today to be magnetar SGR 1900+14 (Mazets et al. 1979a, Mazets & Golenetskii 1981) provided clear evidence of a new class of Galactic high-energy sources.

The neutron-star nature of the SGRs was clear early on. The 8-s pulsations seen in the declining flux tail following the flare from the LMC source, subsequently known as SGR 0526−66, were strongly suggestive of a neutron-star origin (Mazets et al. 1979b), a conclusion supported by the coincidence of the pulsar with the supernova remnant N49 (Cline et al. 1982). The 8-s period was, however, notably longer than that of other young neutron stars like the 33-ms Crab pulsar, and initially an unsteadily accreting neutron star in a binary was thought to be the best explanation for the bursts.

It was not until several years later that the distinct class was fully recognized, when SGRs 0526−66 and 1900+14 were joined by a third Galactic source, SGR 1806−20, which exhibited roughly 100 bursts between 1978 and 1986, with most of the bursts occurring in 1983 (Kouveliotou et al. 1987, Laros et al. 1987).

The magnetar model was born in considering the possibility of amplification of a seed helical magnetic field under dynamo action in a protoneutron star immediately following a core-collapse supernova (Duncan & Thompson 1992). Thompson & Duncan (1995, 1996) demonstrated that SGR phenomena are nicely explained by spontaneous magnetic field decay serving as an energy source for the transient bursts and outbursts as well as for the persistent emission seen in these sources. Their rationale hinged on both neutron-star rotational dynamics and energetics arguments: Given the location of the 8-s pulsar SGR 0526−66 in the LMC supernova remnant N49 (and later noting the central 7-s pulsar in supernova remnant CTB 109), a surface dipolar field strength of order 10^{14}–10^{15} G is required to brake the pulsar from birth periods of a few milliseconds in $\sim 10^4$ years, the typical lifetime of a supernova remnant (see also Paczyński 1992). Furthermore, such a field, particularly if stronger inside the star, could provide a large energy reservoir to explain SGR activity. Thus, multiple lines of reasoning argued for the existence of magnetic field strengths several orders of magnitude larger than had been previously estimated for any radio pulsar or accreting X-ray pulsar. An unambiguous prediction was made: SGR periods must be increasing with time, because so large a field must brake the star on $\sim 10^3$–10^4-year timescales.

In 1998, the first measurement of an SGR spin-down rate was reported (Kouveliotou et al. 1998), and both its sign and magnitude (in this case for SGR 1806−20) provided stunning confirmation of the magnetar model predictions: Under the standard assumption of a magnetic dipole braking, in which the surface dipolar magnetic field strength B is estimated from $B = 3.2 \times 10^{19}\sqrt{P\dot{P}}$ G, a field strength of $\sim 8 \times 10^{14}$ G was inferred. This measurement was followed shortly by an analogous one for SGR 1900+14 (Kouveliotou et al. 1999). The direct measurement of the model-predicted spin-down is what sealed the identification of SGRs as magnetars for most of the astrophysics community.

Meanwhile, a puzzle seemingly unrelated to SGRs was developing. Gregory & Fahlman (1980), using the Einstein Observatory, reported "an extraordinary new celestial X-ray source," a supernova remnant, CTB 109, with a bright X-ray source at the center. Fahlman & Gregory (1981) reported that this source exhibits strong pulsations with a period of 3.5 s (later realized to be the second harmonic of a 7-s fundamental). The discovery of two additional such few-second X-ray pulsars, albeit not in supernova remnants, 1E 1048.1−5937 (Seward et al. 1986) and later 4U

0142+61 (Helfand 1994, Israel et al. 1994), suggested a new source class, as did their unusually soft X-ray spectra. However, such long pulse periods and the unusual spectra were generally interpreted to indicate a new type of low-mass X-ray binary with the pulsations being accretion-powered (e.g., Mereghetti & Stella 1995, Stella et al. 1996). The AXP moniker was introduced by van Paradijs et al. (1995).

Thompson & Duncan (1996) made a crucial suggestion that AXPs may be related to SGRs. Although surprising at the time, from today's hindsight it seems obvious: If AXPs were young neutron stars with a puzzlingly strong energy source and periods of a few seconds, they could well be magnetars as well. Thompson & Duncan remarked, regarding AXPs, "And, in the future, one might expect to detect SGR burst activity from one or more of these objects!"

This expectation was unambiguously confirmed six years later by the discovery of SGR-like bursts from two AXPs (Gavriil et al. 2002, Kaspi et al. 2003). As described later in this review, bursting is now known to be a characteristic property of AXPs, so much so that the line between them and SGRs, for all intents and purposes, no longer exists.

Another key expectation of the magnetar model was that these objects would be prolific glitchers (Thompson & Duncan 1996). Glitches are sudden spin-ups of the neutron star that are commonly observed in young radio pulsars like the Crab pulsar. The discovery of the first magnetar glitch by Kaspi et al. (2000) and the subsequent realization that such events are ubiquitous in these sources and are often—though not always—accompanied by X-ray outbursts (e.g., Dib et al. 2008) are other verifications of magnetar model predictions.

2. OVERVIEW OF THE KNOWN MAGNETAR POPULATION

2.1. Basic Properties

Recently, the first magnetar catalog was published (Olausen & Kaspi 2014) and includes a detailed compendium of the properties of the known magnetars. Here, we summarize these properties and refer the reader for details to that paper or, for the most recent updates, to the online catalog (**www.physics.mcgill.ca/~pulsar/magnetar/main.html**).

The vast majority of known magnetars were discovered via their short X-ray bursts, thanks to sensitive all-sky monitors like the Burst Alert Telescope (BAT) aboard the *Swift Gamma-Ray Burst Mission* and the GBM (Gamma-ray Burst Monitor) aboard the *Fermi Gamma-ray Space Telescope*. These instruments were designed to study GRBs, so they are fine-tuned to finding brief, bright bursts over the full sky. Thus there is strong bias in the known magnetar population toward sources most likely to burst. That nearly all known magnetars share common spin properties and high spin-inferred surface dipolar magnetic fields is a powerful statement regarding which objects in the neutron-star population are burst prone.

In short, apart from the hallmark X-ray activity that defines the class (see Section 3.2.1), magnetars are observed to produce X-ray pulsations in the period range of 2–12 s (ignoring two faster-rotating sources that only briefly exhibited magnetar-like properties; see **Table 1** and Section 2.4). Magnetars are, without exception, spinning down, with spin-down rates that imply spin-down timescales ($\sim P/\dot{P}$) of a few thousand years, suggesting great youth. The spin-down luminosity $\dot{E} \equiv 4\pi^2 I \dot{P}/P^3$, where $I \simeq 10^{45}$ g cm^2 is the stellar moment of inertia, is usually far smaller than the persistent quiescent X-ray luminosity of the sources (see **Table 1**). Moreover, these spin-down rates imply, for 20/23 of the sources for which the spin-down rate has been measured, $B > 5 \times 10^{13}$ G, with the vast majority being over 10^{14} G. Most radio pulsars are thought to be born with periods of at most a few hundred milliseconds; that the shortest known bona fide magnetar has a relatively long 2-s period in spite of a young age is surely a result of rapid magnetic

braking. The long period cutoff of 12 s has been more of a puzzle, which is related to the lifetime of magnetar activity (e.g., Colpi et al. 2000, Viganò et al. 2013). The small observed ranges in P and B are in contrast with a far larger range in quiescent X-ray luminosity, spanning $\sim 10^{30}$ erg s^{-1} up to 2×10^{35} erg s^{-1} in the 2–10-keV band. In fact, the distribution of quiescent luminosities appears to be somewhat bimodal, with the brighter group being the persistent magnetars and the fainter ones the transient magnetars. The latter show greater dynamic range in their outbursts. This large range in luminosity is presently an interesting puzzle, as is the small range in period (see Section 3.1). In the soft X-ray band, magnetar spectra are fairly well described by a blackbody and, in some cases, an additional power-law component, whereas in the hard X-ray band significant spectral hardening occurs such that in some cases the energy spectrum rises, at least as far as has been detected (typically until ~60 keV). Magnetar emission has been seen in some cases at radio, IR, and optical wavelengths.

One source is notable and not included in **Table 1**—the central source of the supernova remnant RCW 103, 1E 161348−5055. It shows a strange 6.67-h X-ray periodicity with a variable pulse profile, as well as repeated large X-ray outbursts (De Luca et al. 2006). D'Aì et al. (2016) and Rea et al. (2016) reported on the discovery of a bright magnetar-like burst from the source, coupled with another large X-ray flux outburst. The source thus bears all the hallmarks of a magnetar, except for the bizarrely long spin period, which cannot be from simple magnetic braking. The long period may be explained by a fall-back disk that slows down the initially faster-rotating neutron star (Li 2007, Ho & Andersson 2017).

2.2. Spatial Distribution

One of the best-determined aspects of magnetars' spatial distribution in the Galaxy is their strict confinement to the Galactic Plane. As shown by Olausen & Kaspi (2014), the scale height of known magnetars is only 20–30 pc in spite of the vast majority of known objects having been discovered through their X-ray bursts by spatially unbiased all-sky X-ray monitors. This scale height is far smaller than that of the radio pulsar population, clearly indicating great youth in magnetars. A 200-km s^{-1} spatial velocity will have moved an object by ~20 pc in 10^5 years. Direct proper motion measurements for magnetars have found a weighted average 200 km s^{-1} with standard deviation 100 km s^{-1} (Tendulkar et al. 2013), which is somewhat lower than that of the radio pulsar population (e.g., Arzoumanian et al. 2002, Brisken et al. 2003, Faucher-Giguère & Kaspi 2006). Thus magnetars typically cannot be much older than 10^5 years and are generally much younger.

The inferred spatial locations within the Galaxy (see **Figure 1**) strongly suggest we are biased against finding more distant magnetars. Nevertheless, some inferred distances that are comparable with that of the Galactic Center indicate that we have been sensitive to a large fraction of the volume of the Milky Way; future all-sky monitors with only modest increases in sensitivity could fully flesh-out the active magnetar population in the Galaxy.

2.3. Associations with Supernova Remnants and Wind Nebulae

Of the 23 confirmed magnetars, 8 are reliably associated with supernova remnant shells, and an additional 2 have possible associations. The large number of remnant associations is fully consistent with the great youth implied both by magnetar spin-down ages and by their proximity to the Galactic Plane. The associated remnants lack unusual properties when compared with shell remnants that harbor neutron stars with lower magnetic fields (Vink & Kuiper 2006, Martin et al. 2014). This appears to be in conflict with the proposal of Duncan & Thompson (1992)

Table 1 Known magnetars and magnetar candidates[a]

Name[b]	P (s)	B[c] (10^{14} G)	Age[d] (kyr)	$\dot{E}$[e] 10^{33} erg s^{-1}	D[f] (kpc)	L_X[g] 10^{33} erg s^{-1}	Band[h]
CXOU J010043.1–721134	8.02	3.9	6.8	1.4	62.4	65	–
4U 0142+61	8.69	1.3	68	0.12	3.6	105	OIR/H
SGR 0418+5729	9.08	0.06	36,000	0.00021	∼2	0.00096	–
SGR 0501+4516	5.76	1.9	15	1.2	∼2	0.81	OIR/H
SGR 0526−66	8.05	5.6	3.4	2.9	53.6	189	–
1E 1048.1–5937	6.46	3.9	4.5	3.3	9.0	49	OIR
(PSR J1119−6127)	0.41	4.1	1.6	2,300	8.4	0.2	R/H
1E 1547.0–5408	2.07	3.2	0.69	210	4.5	1.3	O?/R/H
PSR J1622–4950	4.33	2.7	4.0	8.3	∼9	0.4	R
SGR 1627−41	2.59	2.2	2.2	43	11	3.6	–
CXOU J164710.2–455216	10.6	<0.66	>420	<0.013	3.9	0.45	–
1RXS J170849.0–400910	11.01	4.7	9.0	0.58	3.8	42	O?/H
CXOU J171405.7–381031	3.82	5.0	0.95	45	∼13	56	–
SGR J1745–2900	3.76	2.3	4.3	10	8.3	<0.11	R/H
SGR 1806−20	7.55	20	0.24	45	8.7	163	OIR/H
XTE J1810–197	5.54	2.1	11	1.8	3.5	0.043	OIR/R
Swift J1822.3–1606	8.44	0.14	6,300	0.0014	1.6	>0.0004	–
SGR 1833–0832	7.56	1.6	34	0.32	–	–	–
Swift J1834.9–0846	2.48	1.4	4.9	21	4.2	<0.0084	–
1E 1841–045	11.79	7.0	4.6	0.99	8.5	184	–
(PSR J1846−0258)	0.327	0.49	0.73	8100	6.0	19	–
3XMM J185246.6+003317	11.56	<0.41	>1,300	<0.0036	∼7	<0.006	–
SGR 1900+14	5.20	7.0	0.9	26	12.5	90	H
SGR 1935+2154	3.24	2.2	3.6	17	–	–	–
1E 2259+586	6.98	0.59	230	0.056	3.2	17	OIR/H
SGR 0755−2933	–	–	–	–	–	–	–
SGR 1801−23	–	–	–	–	–	–	–
SGR 1808−20	–	–	–	–	–	–	–
AX J1818.8−1559	–	–	–	–	–	–	–
AX J1845.0−0258	6.97	–	–	–	–	2.9	–
SGR 2013+34	–	–	–	–	–	–	–

[a]All tabulated values from Olausen & Kaspi (2014). A dash indicates no data.
[b]Sources in **bold** have had giant flares. Sources in *italics* are candidates only. Sources in parentheses are normally rotation-powered pulsars.
[c]Spin-inferred magnetic field strength.
[d]Characteristic age from $P/2\dot{P}$.
[e]Spin-down luminosity.
[f]Distance.
[g]Unabsorbed quiescent luminosity in the 2–10-keV band for the distance provided.
[h]H, hard X-rays; O, optical counterpart; OIR, optical/IR counterpart; R, radio counterpart.

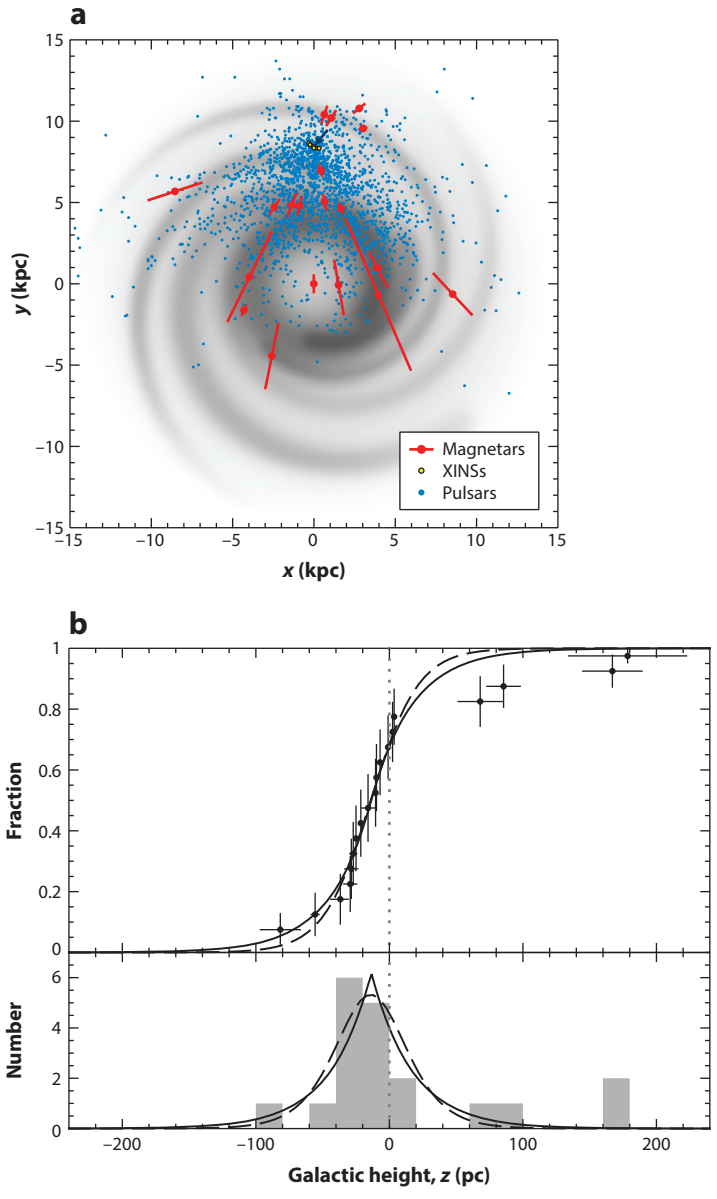

Figure 1

(*a*) Top-down view of the Galaxy, with the Galactic Center at (0,0) and the Sun marked by an arrow. The grayscale shows an estimate for the distribution of free electrons (Cordes & Lazio 2001). Known magnetars are shown as red circles with distance uncertainties indicated, known XINSs are shown as yellow circles, and all other known pulsars are shown as blue dots. (*b*, *top*) Cumulative distribution function of the height z above the Galactic Plane for the 19 known magnetars in the Milky Way. Data are fit to an exponential model (*solid line*) and a self-gravitating, isothermal disc model (*dashed line*). (*b*, *bottom*) Histogram of the distribution in z of the known Galactic magnetars. Lines are as above. Note the offset of the peak from zero; this is the offset of the Sun from the Galactic Plane. Adapted from Olausen & Kaspi (2014) with permission.
Abbreviation: XINS, X-ray isolated neutron star.

that magnetars form from neutron stars rotating with period ∼1 ms at birth, which assists a fast dynamo. The difficulty with this picture is that a neutron star with magnetic field $>10^{14}$ G spinning at 1 ms quickly loses most of its rotational energy, releasing energy in excess of 10^{52} ergs, which is greater than the supernova explosion energy itself. It is therefore likely to be associated with either anomalously large shell remnants, or else no remnant at all, if it expanded sufficiently rapidly to dissipate on a timescale of a few hundred years. The normality of magnetar supernova remnants challenged the dynamo model and led to discussion of strong fossil fields from the progenitor star (Ferrario & Wickramasinghe 2006); however, the latter is not without difficulties (see, e.g., Spruit 2008).

Extended, nebular emission near magnetars, magnetar wind nebulae (MWNe), may exist, in analogy with pulsar wind nebulae (PWNe). PWNe are extended synchrotron nebulae surrounding some radio pulsars, a result of the interaction of relativistic, magnetized pulsar particle winds interacting with their environments, and ultimately powered by the pulsar's rotation [see Gaensler & Slane (2006) for a review]. Observations of an MWN could, in principle, provide important information on the composition and energetics of continuous particle outflows from magnetars. Clear evidence for temporary magnetar outflows has been seen in the form of transient extended radio emission following two giant flares (GFs) (Frail et al. 1999, Gaensler et al. 2005, Gelfand et al. 2005). However interesting, these do not constitute MWNe because the latter by definition are long lived and result from continuous particle outflow even when the magnetar is in quiescence.

There are multiple reports of stable MWNe in the literature (e.g., Rea et al. 2009b, Camero-Arranz et al. 2013); however, extended emission can also be due to dust scattering along the line of sight (e.g., Olausen et al. 2011). Currently the most compelling case of an MWN is an asymmetrical X-ray structure around Swift J1834.9−0846 (Younes et al. 2016). One thing is certain: The phenomenon is not generic to the source class. Deep X-ray imaging observations of many different magnetars have revealed no evidence for any MWN limits (e.g Gotthelf et al. 2004, An et al. 2013). However, Halpern & Gotthelf (2010) report a potential association between a magnetar, CXOU J171405.7−381031, in the supernova remnant CTB 37B, and TeV emission, which they speculate may be a relic MWN.

2.4. Relationship to High-Magnetic-Field Radio Pulsars

If high magnetic fields in neutron stars are responsible for the dramatic X-ray and soft gamma-ray activity in magnetars, and given that some magnetar behavior has been seen in apparently low-*B* sources (such as SGR 0418+5729; Rea et al. 2010), then it stands to reason that high-*B* radio pulsars may occasionally exhibit magnetar-like activity (Kaspi & McLaughlin 2005, Ng & Kaspi 2011). This possibility was also hinted at by higher blackbody temperatures in high-*B* radio pulsars compared with lower-*B* sources of the same age (e.g., Zhu et al. 2011, Olausen et al. 2013). The idea of high-*B* radio pulsars as quiescent magnetars has proven to be correct.

The first example came from the young (age <1 kyr), high-B (5×10^{13} G) but curiously radio-undetected (Archibald et al. 2008) rotation-powered pulsar PSR J1846−0258 in the supernova remnant Kes 75 (Gotthelf et al. 2000). In long-term monitoring designed to measure the source's braking index, Gavriil et al. (2008) detected a sudden X-ray outburst lasting ∼6 weeks and of total energy $\sim 3 \times 10^{41}$ ergs in the 2–10-keV band (see also Kumar & Safi-Harb 2008). The outburst also included several short magnetar-like bursts and a large glitch with unusual recovery (Kuiper & Hermsen 2009, Livingstone et al. 2010). Post-outburst, the source has returned to its quiescent, apparently rotation-powered state, albeit with enhanced timing noise and a significant change in braking index, from 2.65 ± 0.01 pre-outburst to 2.19 ± 0.03 post-outburst (Livingstone

et al. 2011, Archibald et al. 2015a). A second such metamorphosis was seen very recently in PSR J1119−6127, a bona fide radio pulsar, also very young (age <2 kyr) and apparently high-B (4×10^{13} G). In this case the outburst was heralded by bright, magnetar-like X-ray bursts (Göğüş et al. 2016, Kennea et al. 2016, Younes et al. 2016). Follow-up X-ray observations (Archibald et al. 2016a) showed an increase in X-ray flux of nearly a factor of 200 with a dramatic spectral hardening. This outburst was also accompanied by a large glitch (Archibald et al. 2016a) and, remarkably, by a temporary cessation of radio emission (Burgay et al. 2016).

The similarity of the PSR J1846−0258 and PSR J1119−6127 events both to each other and to magnetar outbursts, together with the fact that they are both relatively rare high-B rotation-powered pulsars normally, confirms the close relationship between radio pulsars and magnetars, and the correlation between high spin-inferred magnetic field and magnetar-like activity.

The discovery of radio pulsations from magnetars (see Section 3.3, Camilo et al. 2006, 2007a) also provides an observational link between radio pulsars and magnetars. However, the radio properties of magnetars (see Sections 3.3 and 4.4) are somewhat different from those of conventional radio pulsars.

3. TEMPORAL BEHAVIOR

3.1. X-ray Pulsations, Spin-Down, and Timing

Magnetar X-ray pulse profiles are generally very broad, with one or two components and with duty cycles that approach 100% (see **Figure 2*a***). X-ray pulsed fractions (the fraction of point-source emission that is pulsed) are typically ∼30% but range from ∼10% (Israel et al. 1999) to as high as ∼80% (Kargaltsev et al. 2012). The profile morphologies and pulsed fractions can vary strongly with energy. Pulse profiles are generally stable apart from during outbursts when large profile variations are common. However, there is at least one example of long-term, low-level pulse profile evolution in magnetar 4U 0142+61 (Gonzalez et al. 2010).

Because the X-ray pulsations are generally the most practically observable, long-term timing of magnetars has been done almost exclusively therein, with some inclusions of radio data where available (see Section 3.3). In the past, when X-ray telescope time was very difficult to acquire owing to required long exposures, timing was done by measuring the pulse period at multiple epochs, typically spaced by months to years (e.g., Baykal & Swank 1996, Baykal et al. 2000). This clearly demonstrated regular spin-down in the first known sources, which distinguished them from the accreting X-ray pulsars as these often spin up.

Today, the timing method used most commonly is phase-coherent timing, which is borrowed from the radio pulsar world and was brought first to the magnetar world thanks to the great sensitivity and ease of scheduling of the *Rossi X-Ray Timing Explorer* (RXTE) (Kaspi et al. 1999). In this technique, every rotation of the pulsar is accounted for, sometimes over years, enabling precise measurements of period and eventually spin-down rate. Phase-coherent timing has been accomplished long-term for the five brightest known magnetars using RXTE [see Dib & Kaspi (2014) and references therein] and now *Swift* (e.g., Archibald et al. 2013). Phase-coherent timing has also sometimes been done following magnetar outbursts; however, pulse profile changes, common in outbursts, make this difficult. Moreover, as the source fades, particularly for the transient magnetars that are faint in quiescence, ever-longer integration times are required, often rendering long-term timing impractical.

Phase-coherent timing has enabled very precise measurements of P and $\dot{P}$ now for many magnetars; by the same token, however, deviations from simple spin-down become easily detectable with this technique. In this regard, magnetars are quite prolific. Ubiquitous in their rotational

Figure 2

(*a*) Several X-ray pulse profiles of magnetars in the 1–10-keV band. Courtesy of R.F. Archibald. (*b*) Examples of single bursts from soft gamma repeaters 1806−20 and 1900+14 shown with 7-ms time resolution in the 2–60-keV band from RXTE/PCA data. Adapted from Göğüş et al. (2001) with permission.

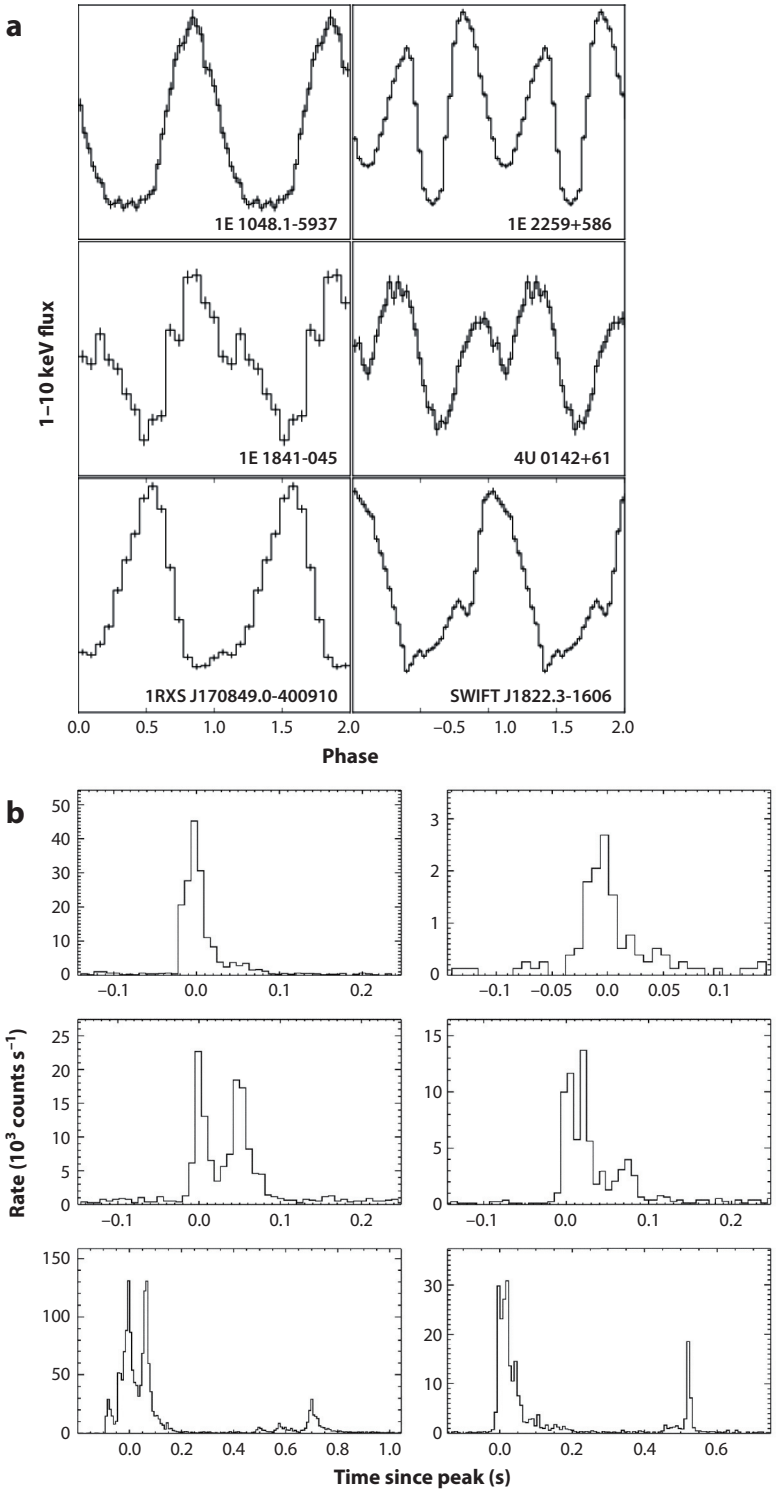

evolution is what is termed timing noise: apparently random wandering of phases particularly on months-to-years timescales. Such wandering is phenomenologically modeled by higher-order derivatives of P (or, equivalently, ν), and in some cases, as many as 10 such derivatives are required (e.g., Dib & Kaspi 2014). However, apart from the smoothly varying wander of timing noise, and thanks to the available timing precision inherent to phase-coherent timing, sudden spin-ups (glitches; and, more rarely, antiglitches) are now observed frequently in magnetars (Section 3.1.1).

Finally, one source shows unusual timing behavior that is worthy of note. 1E 1048.1−5937 has shown episodes of large (by a factor of 5–10) spin-down rate variations that appear to be, curiously, quasi-periodic on a timescale of ∼1,800 days (Archibald et al. 2015b). These episodes have, in all cases observed thus far, followed major flux outbursts, with a delay between the radiative outburst and spin-down fluctuations of ∼100 days. A fourth such flux outburst has very recently begun, at the approximate epoch predicted by the apparent quasi-periodicity (Archibald et al. 2016b).

3.1.1. Glitches. Phase-coherent timing of magnetars by RXTE enabled the discovery that magnetars are among the most frequently glitching neutron stars known (Kaspi et al. 2000, Dib et al. 2008). A glitch, a phenomenon common to young radio pulsars (e.g., Yu et al. 2013), consists of a sudden spin-up, typically involving $\Delta\nu/\nu$ in the range of 10^{-9}–10^{-5} in both magnetars and radio pulsars. Also typically associated with glitches in both radio pulsars and magnetars are long-term changes in spin-down rate $\dot{\nu}$, with typical $\Delta\dot{\nu}/\dot{\nu}$, almost always positive, of at most a few percent and usually far smaller in radio pulsars. A common phenomenon is glitch recovery, in which a sizable fraction of the glitch (in radio pulsars, typically 0–0.5) recovers quasi-exponentially within a week or two following the glitch. A remarkable behavior seen practically exclusively in magnetars is extremely strong glitch recovery, such that the full initial spin-up is recovered, and in some cases over-recovery is seen, such that the overall effect is a spin-down (e.g., Gavriil et al. 2011). These strong recoveries involve initially very large values of $\dot{\nu}$, sometimes upward of 10× the preglitch long-term $\dot{\nu}$ (e.g., Dall'Osso et al. 2003, Kaspi & Gavriil 2003, Kaspi et al. 2003, Woods et al. 2004). Additionally, in one magnetar-like glitch case, the level of timing noise was observed to be greatly enhanced for several years following the over-recovered glitch (Livingstone et al. 2011).

The coincidence of many such glitches and recoveries with large radiative outbursts and their relaxations is suggestive of a magnetospheric phenomenon. Indeed many—though not all—magnetar glitches occur at epochs of large X-ray flux outbursts, which themselves are often accompanied by many outward radiative changes such as short bursts and X-ray pulse profile changes (see Section 3.2.2 below). Curiously some magnetars have only shown radiatively silent glitches (e.g., 1RXS J170849.0−400910; Scholz et al. 2014) and some have shown both silent and loud glitches (e.g., 1E 2259+586; Dib & Kaspi 2014).

Several apparent antiglitches have also been reported in magnetars (Woods et al. 1999, Icdem et al. 2012, Şaşmaz Muş et al. 2014).

These events appear consistent to within the available time resolution with being sudden spin-downs of magnetars and have not been seen in radio pulsars at all. The most convincing of these is the antiglitch reported in 1E 2259+586 (Archibald et al. 2013), in which an apparent sudden spin-down of amplitude $\Delta\nu/\nu \sim 10^{-7}$ accompanied a bright, short X-ray burst and a long-lived flux outburst. Although this event could in principle have resulted from an over-recovered spin-up glitch, the recovery timescale of the initial event would have had to be at most a few days, which is much shorter than any previously observed glitch recovery. The origin of antiglitches is still debated; see Section 5 for further discussion.

3.2. Transient Radiative Behavior: Bursts, Outbursts, Giant Flares, and Quasi-Periodic Oscillations

The term bursts here is used to mean the short, few-millisecond to second events, some of which are followed by longer-lived "tails," an afterglow of sorts. The term outburst is used to describe a sudden but much longer-lived (weeks to months) flux enhancement, which typically involves many of the shorter bursts, and involves a long (many months) tail or afterglow. The term GF is reserved exclusively for what appear to be catastrophic events involving the sudden release of over 10^{44} ergs of energy. Quasi-periodic oscillations (QPOs) have been seen in the tails of some GFs. It is fair to say that nearly all magnetar radiative variability unrelated to their pulsations can be placed into one of these categories.

3.2.1. Bursts. Short bursts are by far the most common type of magnetar radiative event. There are magnetars that have emitted thousands of bursts, usually very much clustered in time, and there are magnetars that, in spite of intensive monitoring programs, have shown at most a handful of bursts. Indeed the former were long thought to be the SGRs of the magnetar population, with the latter being the AXPs. However, with further study it appears that there is a full spectrum in burst rates, and some sources that might originally have been thought to be extremely active (e.g., SGR 0526−66) have lain dormant for decades subsequently (Kulkarni et al. 2003, Tiengo et al. 2009). Similarly, sources that for years were not known to burst (e.g., 1E 2259+586) suddenly entered an active burst phase, emitting several dozen bursts in a few days (Kaspi et al. 2003). This is one key reason the AXP/SGR classification scheme seems obsolete. Note that bursts are more common during outbursts (see Section 3.2.2); however, there are examples of bursts occurring when the source appears otherwise in quiescence (e.g., Gavriil et al. 2002).

There have been multiple detailed statistical studies of the properties of short magnetar bursts (Göğüş et al. 1999, 2000; van der Horst et al. 2012; Lin et al. 2013). Here, we summarize the findings of these studies. Burst peak luminosities can be hyper-Eddington but span a broad spectrum, typically ranging from 10^{36} to 10^{43} erg s^{-1}, with bursts detected right down to the sensitivity limit of current X-ray detectors. Burst durations span over two orders of magnitude, ranging between a few milliseconds and a few seconds, with distributions typically peaking near ∼100 ms. Burst fluence distributions are generally well described with power-law functions of indexes in the range from −1.6 to −1.8 (Göğüş et al. 1999, 2000). Bursts are usually but not always single-peaked, with the rise typically faster than the decay. Interestingly, although some studies have shown that short bursts arrive randomly in pulse phase (e.g., Göğüş et al. 1999, 2000), others have found a preference for bursts near the pulse maximum (e.g., Gavriil et al. 2004). **Figure 2*b*** shows examples of short magnetar bursts.

Some bursts show long, sometimes several-minute tails (e.g., Lenters et al. 2003, Göğüş et al. 2011b, Muş et al. 2015), during which the pulsed flux is sometimes greatly enhanced (e.g., Woods et al. 2005, Mereghetti et al. 2009, An et al. 2014). In this way they are almost like miniature GFs (see Section 3.2.3). Tails fade slowly, with decays well described by relatively flat power laws of indexes well under unity. Though much lower in flux, the long-duration tails can sometimes contain significantly more energy than the burst itself. Ratios of burst-to-tail energies can vary by over an order of magnitude in different sources and even in different bursts in the same source (e.g., Göğüş et al. 2011b).

3.2.2. Outbursts. A magnetar outburst is an event consisting of a large (factor of 10–1,000) and usually sudden increase in the source X-ray flux, sometimes as high as 10^{36} erg s^{-1} [see Rea & Esposito (2011) for a compilation]. These events are generally accompanied by a bevy

of other radiative anomalies such as spectral hardening, change in pulsed fraction, pulse profile changes (often from a simpler to a more complex profile), multiwavelength changes, and multiple short X-ray bursts. Most outbursts for which there are available data also are accompanied by some form of timing anomaly, usually a spin-up glitch or occasionally an antiglitch. The flux following an outburst usually decays on multiple timescales, with a very rapid initial decay within minutes to hours (often missed by observatories) followed by a slower decay (e.g., Woods et al. 2004), sometimes termed an "afterglow," that can last months to years. These slowly fading afterglows are often quasi-exponential (e.g., Rea et al. 2009a) but sometimes have an interesting time evolution, with periods of power-law decays interrupted by periods of a few months of flux stability (e.g., An et al. 2012). In general, magnetar outbursts (even those from the same source) show a variety of timescales for their relaxations (e.g., Esposito et al. 2013). As in the tails of the more common bursts, there is a diversity in the ratios of burst-to-afterglow energies, ranging from a few percent to one to two orders of magnitude (Woods et al. 2004). An example of an X-ray light curve from a magnetar in outburst is shown in **Figure 3**. A description of the spectral evolution of magnetars during and following outbursts is deferred to Section 4 below.

Some sources have shown no outbursts over decades (e.g., 1RXS J1708−4009; Dib & Kaspi 2014), whereas others have had multiple outbursts (e.g., SGRs 1806−20, 1900+14, 1E 1547.0−5408; Woods et al. 2007, Göğüş et al. 2011a, Ng et al. 2011). In the past, AXPs have tended to be associated with sources that have few if any outbursts, whereas SGRs are sources that are much more outburst active. However, in terms of reasonable outburst rate estimates, there is no clear evidence for bimodality, suggesting a full continuum of activity.

The term transient magnetar was introduced to describe those sources that have very low ($<10^{33}$ erg s^{-1}) quiescent luminosities, which generally go unnoticed until they produce outbursts involving flux increases of factors of 100–1,000, accompanied by bright bursts that trigger monitors (e.g., Mori et al. 2013). The first discovered transient magnetar was XTE J1810−197. It was caught in an outburst in 2003 (Ibrahim et al. 2004) and observed to decay on the timescale of a year (Gotthelf & Halpern 2007).

Transient magnetars may in fact be the norm among the magnetar population, with the well-studied bright sources like 4U 0142+61 or 1E 2259+586 being unusual for relatively high quiescent luminosities, upward of 10^{35} erg s^{-1}. Why some magnetars in quiescence are much brighter than most is an interesting question. Some transient magnetars, e.g., SGR 0418+5729 (Rea et al. 2010) or Swift J1822.3−1606 (Rea et al. 2012, Scholz et al. 2014), have low spin-inferred dipole magnetic fields and are thought to possess strong internal toroidal fields.

3.2.3. Giant flares. The queen of magnetar radiative outbursts is the GF. Thus far, only three GFs have been recorded, all from different sources. These events occurred on March 5, 1979 (SGR 0526−66; Evans et al. 1980), August 27, 1998 (SGR 1900+14; Hurley et al. 1999), and December 27, 2004 (SGR 1806−20; Hurley et al. 2005, Mereghetti et al. 2005b, Boggs et al. 2007). These had peak X-ray luminosities in the range of 10^{44}–10^{47} erg s^{-1}, and each was characterized by total energy release of over 10^{44} erg s^{-1} in the X-ray and soft gamma-ray band. The third flare was roughly 100 times more energetic than the first two and was by far the most luminous transient yet observed in the Galaxy; it briefly outshone all the stars in our Galaxy by a factor of 1,000. All three GFs have come from sources traditionally called SGRs, and this one phenomenon appears to be the only behavior that could in principle be used to distinguish SGRs from AXPs; however, SGR 0526−66 has now been inactive for several decades since its GF (Kulkarni et al. 2003, Tiengo et al. 2009), and if it had been discovered during that interval, it probably would have been classified as an AXP.

Figure 3

(*a*) Flux evolution during and after the outburst of 1E 2259+586. Note the initial rapid decrease in flux on the first day, when the vast majority of associated short bursts were detected, followed by the slower subsequent fading. (*b*) Spectral evolution of 1E 2259+586 through and following its 2002 outburst (discussed in Section 4.3). From top to bottom: Unabsorbed flux (2–10 keV), blackbody temperature (kT), photon index, BB radius, and ratio of PL (2–10 keV) to bolometric BB flux. Horizontal dashed lines denote the values of each parameter fortuitously measured one week prior to the outburst. Adapted from Woods et al. (2004) with permission. Abbreviations: BB, blackbody; MJD, modified Julian date; PF, pulsed flux; PL, power law; RXTE, *Rossi X-Ray Timing Explorer*; TDB, barycentric dynamical time; UF, unpulsed flux, XMM, *X-ray Multi-Mirror Mission-Newton*.

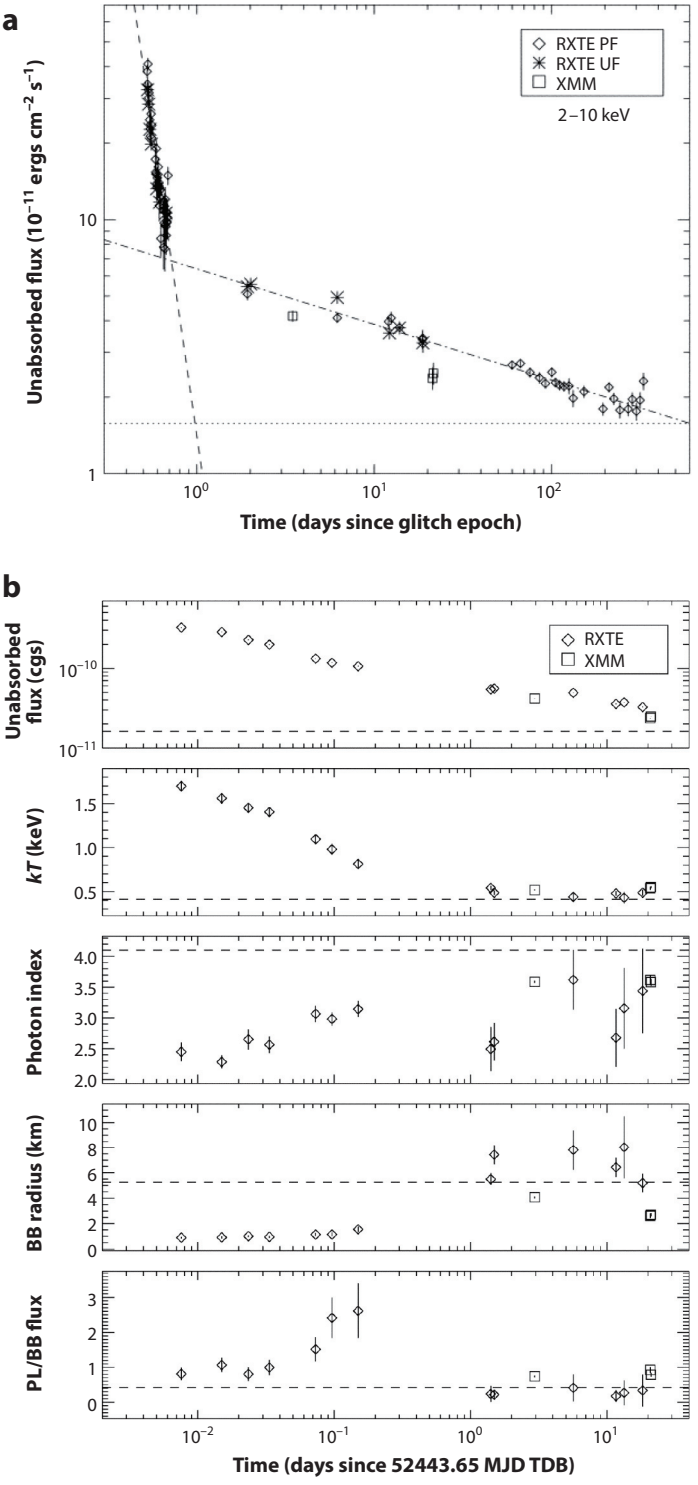

The light curve and effective temperature evolution of the SGR 1806−20 GF is shown in **Figure 4*a*** as an example [see Hurley et al. (2005) for details]. In the initial hard spike, lasting only ∼0.2 s, over 10^{46} ergs were released (assuming a distance of 15 kpc). Its peak luminosity was 10^{47} erg s^{-1}. This spike was followed by a several-minutes-long decay superimposed on which are pulsations at the 7.56-s period of this source. The total fluence in this six-minute tail was 10^{44} ergs.

The enormous peak luminosities observed in the GFs together with their spectral peak in the soft gamma-ray band make them interesting possible counterparts of short, hard GRBs. Hurley et al. (2005) estimated that ∼40% of all short, hard GRBs detected by the BATSE (Burst And Transient Source Experiment) instrument aboard the *Compton Gamma-Ray Observatory* could have been GFs from distant extragalactic magnetars. Ofek et al. (2008) suggested GRB 070201 may have been a GF from a magnetar in M31, and Hurley et al. (2010) suggested another such example, though this interpretation is difficult to confirm in either case. Moreover, young magnetars cannot dominate the short GRB population as the latter are known to be commonly found at large offsets from late-type galaxies (Berger 2014).

3.2.4. Quasi-periodic oscillations. A remarkable phenomenon detected during the pulsating tails of GFs is the high-frequency QPOs. These are believed to be seismic vibrations of the neuton star and may inform us on properties of the stellar interior. These oscillations were first reported in phase-resolved portions of the tail emission of SGR 1806–20 following its 2004 GF (Israel et al. 2005b) at 92.5 Hz (see **Figure 4*b***) and in phase-resolved emission also immediately post-GF in the 1998 event from SGR 1900+14 at 84 Hz (Strohmayer & Watts 2005). Several other QPO frequencies were also reported in these data, which were obtained with RXTE. Similar frequencies from SGR 1900+14 were also seen in *Ramaty High Energy Solar Spectroscopic Imager* data as well as new ones, including a strong 626.5-Hz QPO, again only in specific rotational phase intervals (Watts & Strohmayer 2006). More recently, possible QPOs have also been reported from much fainter bursts from 1E 1547.0–5048 (Huppenkothen et al. 2014); however, these oscillations have proven elusive in other sources (e.g., Huppenkothen et al. 2013).

3.3. Temporal Properties of Low-Frequency Emission

Although every known magnetar has been detected as an X-ray pulsar, small handfuls have had pulsations detected in the optical and radio bands. Optical pulsations have been detected in just three magnetars (Kern & Martin 2002; Dhillon et al. 2005, 2009, 2011). The optical pulses seen thus far are comparably broad and similar to the corresponding X-ray pulse profile, at least within the limited optical statistics. Importantly, all are detected with high pulsed fractions ranging from 20% to 50%, in one case higher than that in X-rays (Dhillon et al. 2011). This is strongly suggestive of a magnetospheric origin (see Section 5). Only three have had optical pulsations detected, and six more have shown optical and/or IR emission not yet seen to pulse (**Table 1**). The overall picture of the relationship of the IR emission to the X-rays remains unclear. In several cases, clear IR enhancements have been noted at the time of outbursts, often with the IR correlated with the X-rays (Rea et al. 2004, Tam et al. 2004, Israel et al. 2005a). However, in some cases, no correlation has been seen (Durant & van Kerkwijk 2006, Tam et al. 2008, Testa et al. 2008, Wang et al. 2008).

Radio pulsations have now been detected in four magnetars (Camilo et al. 2006, 2007a; Levin et al. 2010; Eatough et al. 2013; Shannon & Johnston 2013), five if counting the recent magnetar-like outburst from the radio pulsar PSR J1119−6127 (Archibald et al. 2016a). All four are transient magnetars, and their radio emission is transient too and associated with an X-ray outburst. In XTE J1810−197 (the first detected radio-emitting magnetar), pulsations were observed after, but not

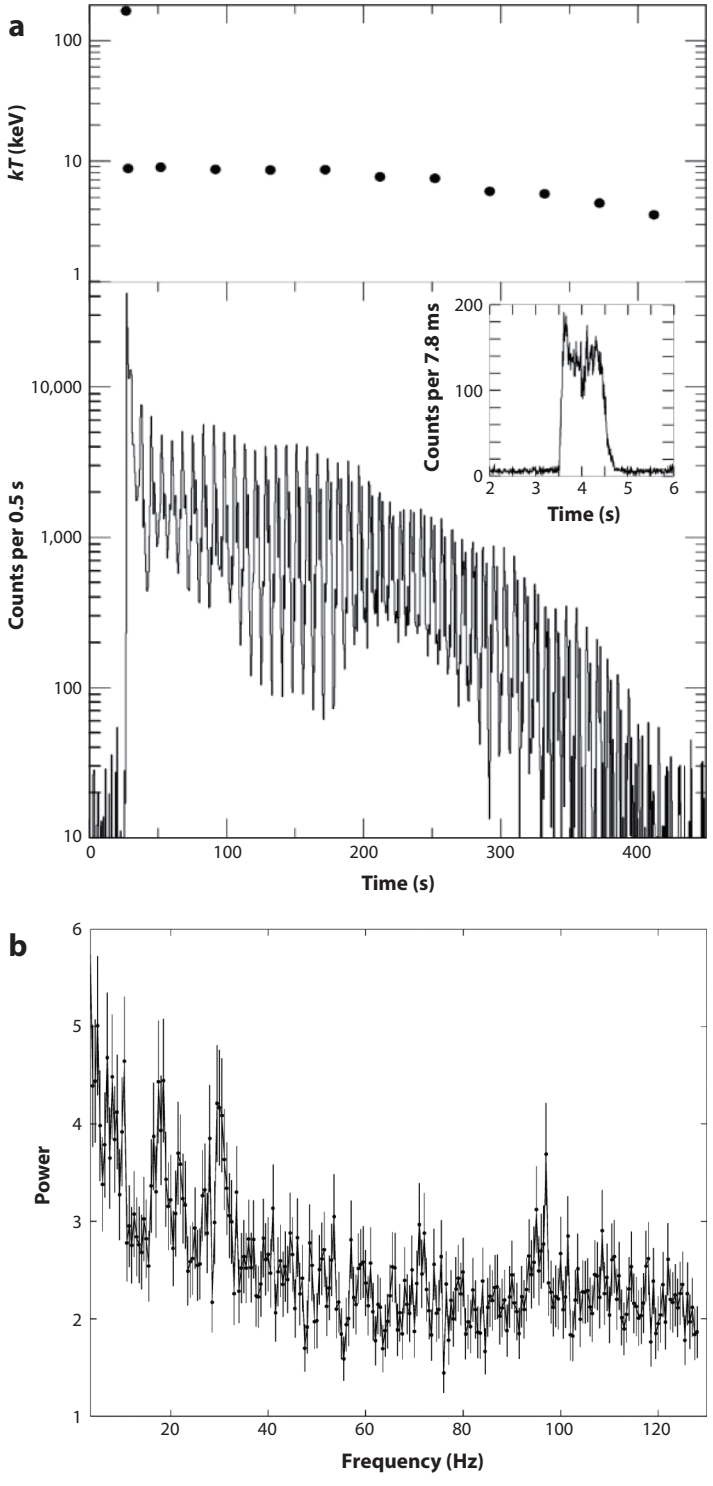

Figure 4

(*a*) The 2004 giant flare from SGR 1806–20. (*Bottom*) 20–100-keV time history with 0.5-s resolution from the RHESSI satellite, showing the initial spike (which saturated the detector) at 26 s. The inset shows a precursor burst that occurred just prior (with 8-ms resolution). The oscillations in the decaying tail are at the neutron-star rotation period. (*Top*) Blackbody temperature of the emission. Adapted from Hurley et al. (2005) with permission. (*b*) Power spectrum of the SGR 1806–20 giant flare 2–80-keV light curve in the interval 200–300 s. Two low-frequency peaks at ~18 and ~30 Hz are visible, together with a small excess at ~95 Hz. Adapted from Israel et al. (2005b) with permission.

before, its 2003 outburst. The radio pulsations disappeared in late 2008 with no prior secular decrease in radio flux (Camilo et al. 2016). Behavior in the other sources is similar (Camilo et al. 2007a, Levin et al. 2012). The persistent (i.e., nontransient) magnetars and several other transient magnetars have been searched for radio pulsations but with no detections (e.g., Lazarus et al. 2012, Tong et al. 2013b). In the four magnetars with confirmed radio pulsations, the radio emission in all cases is very bright and shows large pulse-to-pulse variability, with pulse morphologies, both single and average, that can be broad and that generally change enormously on timescales of minutes. They can be punctuated by spiky peaks that can be much shorter than the pulse period. This radio emission is also highly linearly polarized, with polarization fractions of 60–100%. No evidence for a radio burst at the epoch of a GF has been seen (Tendulkar et al. 2016).

One radio-detected magnetar, SGR 1745−2900, is located in the Galactic Center (Eatough et al. 2013, Kennea et al. 2013, Mori et al. 2013, Shannon & Johnston 2013). The radio properties of the magnetar are similar to those of the first three, with evidence for independent X-ray/radio flux evolution (Lynch et al. 2015, Torne et al. 2015). Notable is the far lower than expected interstellar scattering (Bower et al. 2014, Spitler et al. 2014). This is exciting as it suggests renewed hope for finding radio pulsars for dynamical studies near Sgr A* and for constraining properties of the Sgr A* accretion disk (Eatough et al. 2013).

4. RADIATION SPECTRUM

4.1. Burst Spectra

The spectra of magnetar bursts contain important information regarding the physics underlying these events. Here, we consider spectra, dividing bursts into two main categories: short bursts (see Section 3.2.1) and giant flares (see Section 3.2.3).

4.1.1. Short bursts. Bursts are generally spectrally much harder than the persistent X-ray emission from magnetars and, though easily detectable below 10 keV, peak above that energy. Hence, they are best studied by broadband X-ray instruments or by combining simultaneous data from multiple instruments, if possible. Multiple different models have been used to describe burst spectra, including a simple blackbody, double blackbodies, OTTB (optically thin thermal bremsstrahlung) models, or Comptonization models (a power law with an exponential cutoff). Even with very broadband spectra (e.g., 8–200 keV) it is hard to distinguish among these models (e.g., van der Horst et al. 2012); moreover, sometimes the overall spectra of bursts in a cluster change with epoch (e.g., von Kienlin et al. 2012). Regardless of model, in all studies, spectral hardness is found to be related to burst fluence. In most cases the two appear anticorrelated (Göğüş et al. 1999, 2000, 2001; van der Horst et al. 2012), though in some cases they are correlated (Gavriil et al. 2004). Tail spectra are typically well modeled by blackbodies that show decreasing kT at constant radius (e.g., Göğüş et al. 2011b, An et al. 2014).

Curiously, an apparent emission feature near ∼13 keV has been noted in the spectra of bright magnetar bursts detected with RXTE/PCA in the sources 1E 1048.1−5937, 4U 0142+61, and XTE J1810−197 (Gavriil et al. 2002, 2011; Woods et al. 2005; Chakraborty et al. 2016). These features are variable, occurring transiently during the burst evolution, but are not subtle: They are easily visible by eye, with equivalent widths of ∼1 keV. Although it is tempting to argue these features are of some unknown instrumental origin (even though they are not always seen in RXTE magnetar burst data), An et al. (2014) found evidence of them in *Nuclear Spectroscopic Telescope Array* (NuSTAR) data from 1E 1048.1−5937, which happened to burst during an observation. The origin of these burst features is unknown; if they are from some form of cyclotron emission,

it is unclear why all the sources in which these features have been observed show them near the same energy, because presumably they have a variety of field strengths in the emission region. There is no spectral line known with that energy.

4.1.2. Giant flares. Described in Section 3.2.3, the initial brief spike seen in magnetar GFs is extremely hard, peaking in the soft gamma-ray band and extending at least to megaelectronvolt energies. It is followed by a softening on timescales of seconds to minutes. In **Figure 4**, where the 2004 GF of SGR 1806–20 is shown, a blackbody describes the data reasonably well, and the initial kT is ∼175 keV (Hurley et al. 2005, Boggs et al. 2007). Following the spike was a few-seconds decay whose spectrum was nonthermal, which was described by a power law of index $\Gamma \sim 1.4$, and then a series of pulsations at the 7.5-s spin period, with spectra consisting of a combination of blackbody and power-law emission. Both softened over the next few minutes, from $kT \simeq 11$ keV to 3.5 keV and $\Gamma \simeq 1.7$ to 2 for the two components, respectively. Similar initial and subsequent spectra were seen in the 1998 GF from SGR 1900+14 (Hurley et al. 1999). Although at the peak of the 1979 GF from SGR 0526−66 the spectrum may have been slightly softer than in the latter two cases (the best estimate is ∼30 keV), the overall trend of a very hard spike and subsequent softening were also seen (Fenimore et al. 1981). In some ways, GF spectral evolution mirrors that of the X-ray emission in less-energetic magnetar outbursts: sudden hardening and subsequent softening (see Section 4.3).

4.2. Persistent Emission

The X-ray spectra of magnetars in quiescence fall into two broad classes: those in high-quiescent-luminosity sources (the persistent magnetars) and those in low-quiescent-luminosity sources (the transient magnetars). The observational distinction is based both on quiescent luminosity ($\gtrsim 10^{33}$ erg s^{-1} for persistent sources like 1E 2259+586 or 4U 0142+61 versus $\lesssim 10^{33}$ erg s^{-1} for transient sources like XTE J1810−197 or SGR J1745−2900) and on flux dynamic range in outbursts (factor of $\lesssim$100 in persistent sources versus $\gtrsim$100 in transient sources).

Classic magnetars in quiescence show multiple-component X-ray spectra that are usually well parameterized in the 0.5–10-keV band by an absorbed blackbody of $kT \simeq 0.3$–0.5 keV plus a power-law component of photon index in the range from −2 to −4 [see Olausen & Kaspi (2014) for a compilation]. An example of such a spectrum is shown in **Figure 5*a***. Typically the nonthermal component begins to dominate the spectrum above ∼3–4 keV. At least qualitatively, the thermal component is thought to arise from the hot neutron-star surface, whereas the power-law tail likely arises from a combination of atmospheric and magnetospheric effects. Typically the power law dominates energetically by at least a factor of two, although in the soft X-ray band this quantity depends strongly on the absorption, because $N_{\rm H}$ and kT are generally highly covariant. Double blackbodies can often fit magnetar spectra as well and, in rare cases, double power laws. Note, however, as described in Section 5, the soft-band X-ray spectrum is thought to arise physically from a complicated blending of surface thermal emission distorted by the presence of a highly magnetized atmosphere, then Comptonized by currents in the magnetosphere that can themselves result in surface heating via return currents. Hence the simple, e.g., blackbody plus power-law or double-blackbody, parameterizations should be seen as merely convenient and readily available (i.e., in `XSPEC`) descriptions of the data rather than actual measurements of physical properties.

Observations using INTEGRAL (*International Gamma-Ray Astrophysics Laboratory*) and the RXTE led to the surprising discovery just over a decade ago that for persistent magnetars, the spectrum turns up above 10 keV, such that the bulk of their energy comes out above the traditional 0.5–10-keV band (Kuiper et al. 2004, 2006). This prominent hard spectral component is shown for

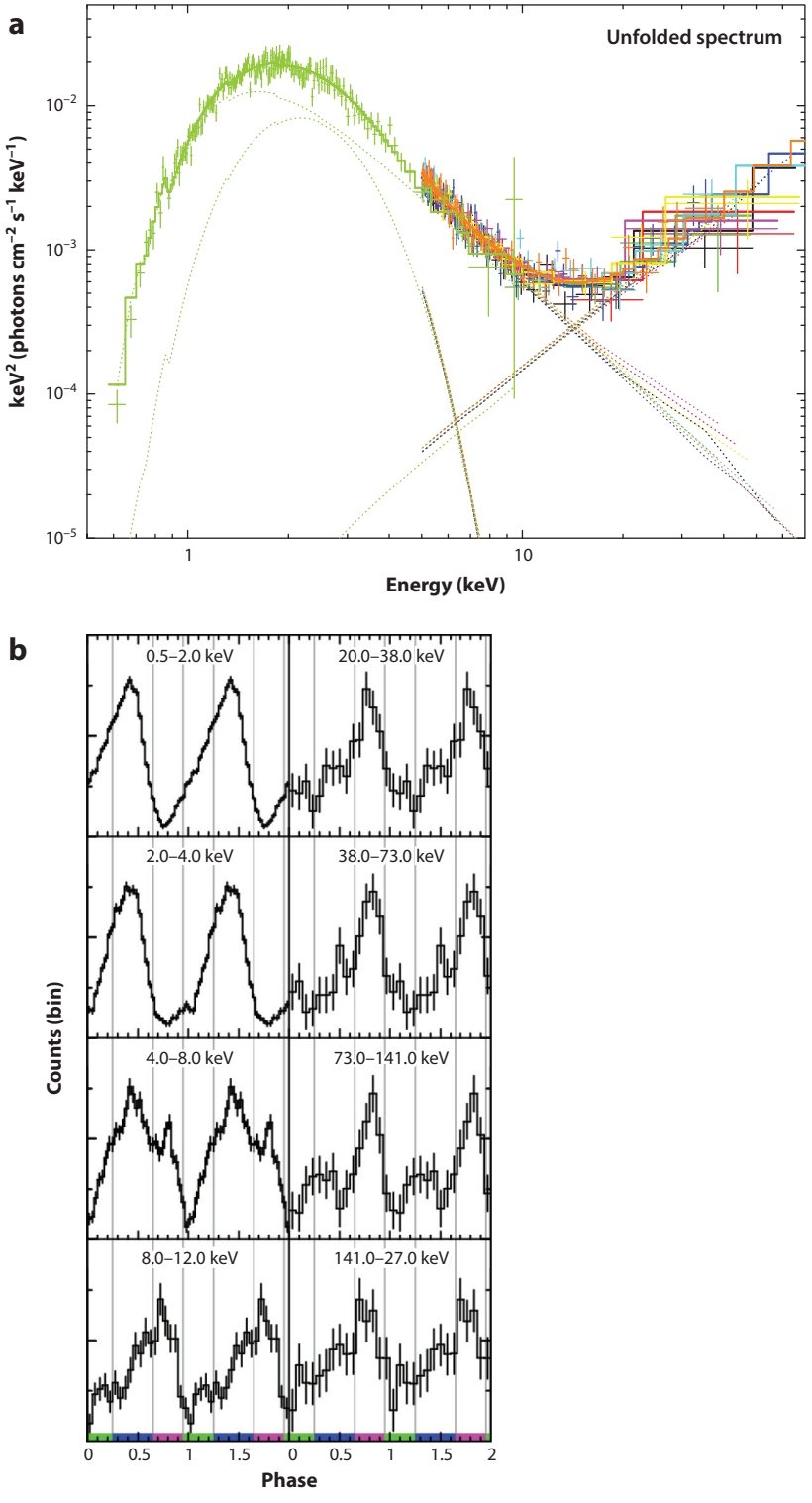

Figure 5

(*a*) Broadband phase-averaged X-ray spectrum from combined *Swift*/XRT (*green*) and NuSTAR observations of 1E 2259+586. Adapted from Vogel et al. (2014) with permission. The best-fit model of an absorbed blackbody plus two power laws is shown. The spectral turn up in this source near 15 keV is obvious. (*b*) Pulse profiles in different X-ray energy bands for 1RXS J170849–400910. Adapted from den Hartog et al. (2008a) with permission.

magnetar 1E 2259+586 in **Figure 5*a***. Such hard components have been seen now in six sources in quiescence. Kaspi & Boydstun (2010) and Enoto et al. (2010) reported a possible anticorrelation between the degree of spectral up-turn and spin-down rate and/or spin-inferred magnetic field strength, such that higher spin-inferred B sources show little to no spectral up-turn (Mereghetti et al. 2005a, Götz et al. 2006).

Another remarkable feature of magnetar spectra is that they are highly rotational-phase dependent (den Hartog et al. 2008a,b). This is diagnosed in two different ways: by strong energy dependence of the pulse profile as shown for magnetar 1RXS J170849−400910 in **Figure 5*b***, or, equivalently, as variations in fitted spectral parameters with rotational phase. The latter is detected generically. The strong phase variation is expected for magnetospheric emission beamed along magnetic field lines and has been used to deduce constraints on the geometry of the hard X-ray source (Hascoët et al. 2014, Vogel et al. 2014, An et al. 2015, Tendulkar et al. 2015). This is discussed in detail in Section 5.

Transient magnetars in quiescence show X-ray spectra that are consistent with being pure absorbed blackbodies, with $kT \simeq 0.15$–0.3 keV [see Olausen & Kaspi (2014) for a compilation]. As these sources are generally discovered in outburst, measuring quiescent spectra and temperatures requires waiting months to years until the source returns to a quiescent state (e.g., Alford & Halpern 2016). Phase-resolved spectroscopy for transient magnetars in quiescence has yet to be done owing to the faintness of the sources. In these objects, the nonthermal magnetospheric processes responsible for the power laws seen in persistent magnetars seem absent, in spite of the spin properties of the two classes being similar, though sensitivity may play a role. Interestingly, quiescent transient magnetar spectra are similar to the X-ray spectra of some high-B radio pulsars (see Section 2.4).

4.3. X-ray Spectral Evolution in Outburst

The spectra of magnetars change dramatically at times of outburst, generically hardening initially, then slowly softening as the flux relaxes back to quiescence over typically months to years. The flux evolution in outbursts was discussed in Section 3.2.2, with an example shown in **Figure 3*a***. The hardening at outburst, for a spectrum parameterized by an absorbed blackbody plus power law, can generally be described by an initial increase in kT by a factor of ∼2–3 (often, but not always, with a decrease in effective blackbody radius by a factor of a few), together with a decrease in photon index by a factor of ∼2. These quantities then relax back to their quiescent values on the same timescale as the flux relaxation. An example of the spectral evolution seen in one magnetar (1E 2259+586) outburst is shown in **Figure 6**. The hardness/flux correlation seen in magnetar outbursts is thought to be closely related to the correlation between hardness and spin-down rate noted by Marsden & White (2001), in that all these quantities are related to the degree of magnetospheric twist, with larger twists corresponding to higher luminosities, spin-down rates, and hardness.

There is, however, considerable diversity in the spectral changes and evolution post-outburst. Just as relaxation light curves for different sources can look very different, the degree of hardening and the manifestation of that hardening (be it a greater increase in kT or decrease in photon index) vary from outburst to outburst (Rea & Esposito 2011). In the first-discovered transient magnetar, XTE J1810−197, for example, Gotthelf & Halpern (2007) found that the spectrum was well described by two blackbodies, each of which had its luminosity decay on exponential timescales, albeit different ones (870 and 280 days); this behavior is not reproduced in most other sources. Even for the same source, outbursts can show a variety of behaviors (Israel et al. 2010, Ng et al. 2011, Kuiper et al. 2012a). Scholz & Kaspi (2011) show that there does not appear to

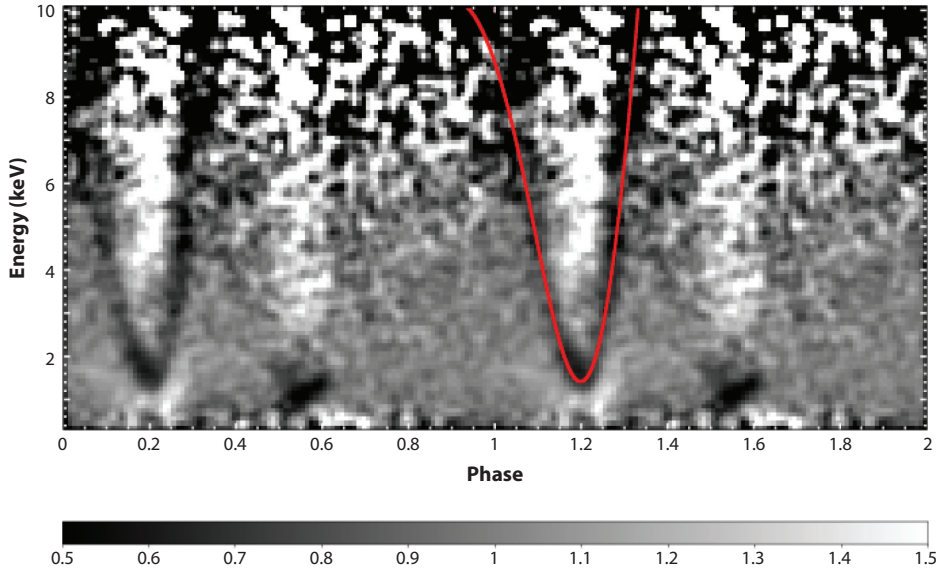

Figure 6

Phase-resolved spectroscopy of SGR 0418+5729. The spectral flux is shown in the energy versus phase plane for XMM-Newton/EPIC data. The image was obtained by binning the EPIC source counts into 100 phase bins and 100-eV-wide energy channels and dividing these values first by the average number of counts in the same energy bin (corresponding to the phase-averaged energy spectrum) and then by the relative 0.3–10-keV count rate in the same phase interval (corresponding to the pulse profile normalized to the average count rate). The red line shows (for only one of the two displayed cycles) a simple proton cyclotron model. Adapted from Tiengo et al. (2013) with permission.

exist a universal law linking the degree of flux increase over the quiescent level with the degree of flux hardening. By contrast, Beloborodov & Li (2016) showed a relationship between X-ray luminosity and inferred blackbody emitting area during outburst relaxations of seven different magnetars, which is consistent with theoretical predictions based on j-bundle untwisting (see Section 5).

Tiengo et al. (2013) reported the presence of a feature—an absorption line—in the outburst X-ray spectrum of SGR 0418+5729, the source with low spin-inferred magnetic field (Rea et al. 2010). The energy of the line apparently varies strongly with pulse phase; see **Figure 6**. The variation in energy is roughly a factor of five over just 10% of the pulse phase. Those authors interpret the line as a proton cyclotron feature; its energy implies a magnetic field ranging from 2×10^{14} G to more than 10^{15} G. If interpreted as an electron cyclotron line, however, the implied field is 2,000× lower. If the proton cyclotron interpretation is correct, this observation strongly supports the hypothesis that SGR 0418+5729 has a far stronger field than is inferred from the dipolar component. A similar phase-dependent absorption line was recently reported by Rodríguez Castillo et al. (2016) for the magnetar Swift J1822.3−1606. This is particularly interesting as this source has the second lowest spin-inferred B field of the known magnetars (Rea et al. 2012, Scholz et al. 2014, Rodríguez Castillo et al. 2016). Why the two lowest-inferred B sources should be the only ones with such phase-dependent features is unclear. The emission may come from a magnetic loop near the surface of the star, wherein the field energy is appropriate for the line to be in the observed spectral window.

4.4. Low-Frequency Emission

As discussed in Section 3.3, six magnetars have had optical or IR emission detected. One is bright enough to have had its optical/IR spectrum studied in detail: 4U 0142+61 (Wang et al. 2006). The optical/IR emission is well described by a power law of index 0.3 and is presumed to be magnetospheric, in line with the detection of strong optical pulsations (Kern & Martin 2002, Dhillon et al. 2005). However, the IR *Spitzer*-measured 4.5- and 8.0-μm emission deviates from this function and can be well described by blackbody emission for a temperature of 920 K. Wang et al. (2006) interpreted this near-IR emission as arising from an X-ray heated dust disk that is a remnant of material that fell back toward the newly born neutron star following the supernova. However, this interpretation is not unique; it may also be some form of nonthermal magnetospheric emission. The detection of pulsations in the near-IR would be key as these are not expected at more than the few-percent level for a disk. Note that Wang et al. (2008) did deep *Spitzer* observations of magnetar 1E 1048.1−5937 that appear to rule out any IR emission similar to that in 4U 0142+61 and hence challenge the disk interpretation.

The spectrum of the pulsating radio emission seen at least transiently from four magnetars is remarkably flat (Camilo et al. 2007a,b; Lazaridis et al. 2008; Levin et al. 2010). This is true even over a wide range of radio frequencies (e.g., 1.4–45 GHz for 1E 1547.0−5408; Camilo et al. 2008). This flatness is in contrast to the spectra of rotation-powered pulsars, which are typically steep, with negative spectral indexes of ∼−1.8 (e.g., Maron et al. 2000). Magnetar SGR J1745−2900 has been detected at frequencies as high as 225 GHz, the highest yet for any pulsar (Torne et al. 2015). However, for this same source, Pennucci et al. (2015) reported a steep spectral index (−1.4) between 2 and 9 GHz. Although overall approximately flat, magnetar radio spectra may not be well described by a single spectral index. Measurement of the broadband radio spectra is challenging because of the high variability and the common presence of terrestrial interference at relevant timescales.

5. MECHANISM OF MAGNETAR ACTIVITY

5.1. Internal Dynamics

A nascent magnetar experiences fast evolution in the first minutes of its life. Magnetohydrodynamic (MHD) relaxation leads to a magnetic configuration that has a strong toroidal component (Braithwaite 2009), whose stability is assisted by compositional stratification (Akgün et al. 2013). Neutrino cooling leads to crystallization of the crust. The resulting object has a liquid core of radius $R \sim 10$ km surrounded by a 1-km-thick solid crust.

The subsequent behavior of magnetars on the timescales of 1–10 kyr is associated with slow evolution of the magnetic field inside the star, which is capable of breaking the solid crust. The interior of a neutron star is an excellent conductor, and hence the magnetic field is practically "frozen" in the stellar material. More precisely, the magnetic field is frozen in the electron fluid, and field evolution is possible because of the multifluid composition of the star. The electrons may slowly drift with respect to neutrons and also with respect to ions. This gives two processes capable of moving the magnetic field lines: ambipolar diffusion and Hall drift (Goldreich & Reisenegger 1992).

5.1.1. Ambipolar diffusion. Ambipolar diffusion is the motion of the electron–proton plasma (coupled with the magnetic field) through the static neutron liquid in the core. The magnetar is born with electric currents, $\mathbf{j} = (c/4\pi)\nabla \times \mathbf{B}$, and hence Lorentz forces $\mathbf{j} \times \mathbf{B}/c$ are applied

to the plasma. The plasma does not move in a young hot magnetar—it is stuck in the heavy neutron liquid owing to frequent proton–neutron (p-n) collisions. As the star ages and cools down, the p-n collision rate decreases (Yakovlev & Shalybkov 1990), and ambipolar drift develops on the timescale $t_{\rm amb} \sim 10^3 (T_9/k_{-5}B_{16})^2$ years (hereafter, we use the standard notation X_m for a quantity X normalized to 10^m in centimeter–gram–second units), where the wave number $k \sim 10^{-5}$ cm^{-1} describes the gradient of the magnetic field in the core and corresponds to a characteristic scale $\pi/k \lesssim R$. The timescale of ambipolar diffusion becomes comparable with the star's age when the core temperature decreases to $\sim 10^9$ K. Then a significant drift occurs and a large fraction of magnetic energy can be dissipated by the p-n friction. As the drift develops, it generates plasma pressure gradients, which tend to be erased by weak interactions $e + p \leftrightarrow n$ (Goldreich & Reisenegger 1992, Thompson & Duncan 1996). Core superfluidity is capable of suppressing these processes and quickly ending ambipolar diffusion (Glampedakis et al. 2011). However, for a plausible critical temperature of superfluidity, the suppression effect is moderate, and ambipolar diffusion can still be the main cause of magnetar activity (Beloborodov & Li 2016). The ambipolar drift tends to relax the magnetic stresses that drive it and eventually stalls while the core temperature drops.

5.1.2. Hall drift. Hall drift is the transport of magnetic field lines by the electric current $\mathbf{j}$, which implies a flow of the electron fluid relative to the ions with velocity $\mathbf{v}_{\rm H} = -\mathbf{j}/en_e$, where n_e is the electron density. Hall drift is normally very slow in the core, because of its high density $n_e \sim 10^{37}$ cm^{-3}, but can be significant in the crust.

Hall drift conserves the total magnetic energy; however, it can generate new electric currents. When ohmic dissipation is taken into account, the evolution may come to a steady state (Gourgouliatos & Cumming 2014). The field evolution in the crust was simulated numerically for axisymmetric configurations (e.g., Pons et al. 2009) and in more general 3D configurations (Gourgouliatos et al. 2016). It was seen to build up strong elastic stresses in the crust (Perna & Pons 2011). Hall waves can also be excited near the crust-core boundary (Thompson & Duncan 1996).

5.1.3. Mechanical failures of the crust. The ambipolar diffusion and Hall drift of the magnetic field lines result in the gradual accumulation of crustal stresses, which can trigger surface motions in magnetars. The crust is nearly incompressible; however, its Coulomb lattice can yield to shear stresses. Thompson & Duncan (1995) proposed the picture of "starquakes"—sudden fractures and displacements of the crust, which shake the magnetosphere and trigger bursts. Cracks involving void formation are impossible in a neutron-star crust because of the huge hydrostatic pressure (Jones 2003), and slips are forbidden by the strong magnetic fields unless the slip plane is aligned with the magnetic flux surfaces (Levin & Lyutikov 2012). A plausible yielding mechanism is a plastic flow. It is triggered when the elastic strain exceeds a critical value $s_{\rm cr} \lesssim 0.1$, where the maximum value of $s_{\rm cr} \sim 0.1$ describes the strength of an ideal crystal. The lattice failure was demonstrated on the microscopic level using molecular dynamic simulations (Horowitz & Kadau 2009, Chugunov & Horowitz 2010).

A growing magnetic stress may be applied from the evolving core and reach the maximum elastic stress $s_{\rm cr}\mu$, where $\mu \sim 10^{30}$ erg cm^{-3} is the shear modulus of the lower crust; then the crust will experience a shear flow. Magnetic stresses can also be generated in the crust itself, due to Hall drift (Thompson & Duncan 1996, Perna & Pons 2011). This leads to a thermoplastic instability (Beloborodov & Levin 2014), which launches thermoplastic waves, relieving the stress. The propagating wave burns magnetic energy, resembling the deflagration front in combustion physics. Its speed is $v \sim (\chi B^2/4\pi\eta)^{1/2}$, where $\chi \sim 10$ cm^2 s^{-1} is the heat diffusion coefficient and

η is the viscosity coefficient of the plastic flow. Crustal flows are capable of releasing significant magnetic energy (e.g., Lander et al. 2015) with a complicated temporal pattern.

5.1.4. Observational signatures of internal instabilities. Internal dynamics of magnetars shape their observational properties in three basic ways: (*a*) glitches in the rotation rate, (*b*) internal heating and increased surface luminosity, and (*c*) twisting of the external magnetosphere. This leads to rich phenomenology of magnetar activity, as described in Sections 2–4, from GFs to timing anomalies to persistent hard X-ray emission and hot spots on the magnetar surface. Here, we briefly discuss internal glitches; mechanisms of internal heating and magnetospheric phenomena are described in Sections 5.2–5.4.

A common internal mechanism for glitches in pulsars is related to neutron superfluidity (Anderson & Itoh 1975). The magnetospheric spin-down torque is applied to the crustal lattice and not directly to the free neutrons that dominate the star's moment of inertia. Neutrons in the lower crust are expected to form superfluid and their spin down can lag behind; i.e., the neutrons rotate slightly faster than the crustal lattice. Vorticity of the neutron superfluid is quantized into vortex lines, and the lag is the consequence of the vortices being pinned to the lattice nuclei. When the vortices become unpinned, they are allowed to move away from the rotation axis and the superfluid can spin down; its angular momentum is passed to the lattice in this event, producing a spin-up glitch. Thompson & Duncan (1996) argued that sudden starquakes can cause such unpinning. Alternatively, the superfluid vortices can be unpinned because of a heating episode (Link & Epstein 1995), and this is expected to occur in a thermoplastic wave.

5.2. Internal Heating and Surface Emission

Heat that is initially stored in a nascent neutron star is eventually lost to neutrino emission and surface radiation. As a result, a thousand-year-old neutron star is normally expected to have an internal temperature $T_{\rm core} \sim 10^8$ K and a surface temperature $T_{\rm s} \sim 10^6$ K (Yakovlev & Pethick 2004), which corresponds to a surface luminosity $L_{\rm s} \sim 10^{33}$ erg s^{-1}. In contrast, the surface luminosities of classical active magnetars are around $L_{\rm s} \approx 10^{35}$ erg s^{-1}. For a neutron star of radius $R \approx 10$–13 km, this luminosity corresponds to effective surface temperature $T_{\rm s} = (L_{\rm s}/4\pi R^2\sigma_{\rm SB})^{1/4} \approx 4 \times 10^6$ K, where $\sigma_{\rm SB}$ is the Stefan–Boltzmann constant. This indicates that magnetars are strongly heated by some mechanism.

5.2.1. Heating of the core. The high surface luminosity may be associated with a strong heat flux from the core, which implies an unusually high $T_{\rm core}$ (Thompson & Duncan 1996). A steady heat flux to the surface is established on the conduction timescale of 1–10 years, which is much shorter than the magnetar age. Then the steady heat diffusion determines the relation between $T_{\rm core}$ and $T_{\rm s}$. The main drop of temperature from $T_{\rm core}$ to $T_{\rm s}$ occurs in the blanketing envelope in the upper crust, in particular where $\rho < 10^9$ g cm^{-3} (Yakovlev & Pethick 2004). The $T_{\rm core}$–$T_{\rm s}$ relation depends on the magnetic field $\mathbf{B}$ in the blanket and its chemical composition (Potekhin et al. 2003). Increasing the core temperature above $\sim 10^9$ K does not increase $L_{\rm s}$ because the heat flux is lost to neutrino emission on its way through the crust (Potekhin et al. 2015b). Thus $L_{\rm s} \sim 10^{35}$ erg s^{-1} is naturally obtained for any $T_{\rm core} \gtrsim 10^9$ K.

However, the ability of magnetars to sustain $T_{\rm core} \sim 10^9$ K for 1–10 kyr is questionable. At such high temperatures, huge neutrino losses are expected in the core itself (Yakovlev & Pethick 2004). A minimum neutrino cooling rate is found in nonsuperfluid cores due to modified Urca reactions, $\dot{q}_\nu \sim 10^{21} T_9^8$ erg cm^{-3} s^{-1}. A possible transition to superfluidity at a critical temperature $T_{\rm crit} \gtrsim 10^9$ K would only increase the cooling rate, as a result of continual breaking and formation

of Cooper pairs (Flowers et al. 1976). In general, only a very powerful heat source can compete with neutrino losses at $T_{\rm core} \sim 10^9$ K. A recent analysis by Beloborodov & Li (2016) shows that heating by ambipolar diffusion may sustain the observed surface luminosity $L_{\rm s} \sim 10^{35}$ erg s^{-1} if the internal magnetic field is ultrastrong, $B \gtrsim 10^{16}$ G, but only for a time shorter than 1 kyr.

5.2.2. Heating of the crust. An alternative scenario of internal heating assumes a cool core and a heat source in the crust. Then the radial temperature profile $T(r)$ peaks in the crust. Most of the heat is conducted to the core and lost to neutrino emission; however, a fraction reaches the stellar surface and could power the observed $L_{\rm s}$. Requirements of this scenario were investigated by Kaminker et al. (2014). They placed a phenomenological heat source at various depths without specifying its mechanism and found that sustaining the surface luminosity $L_{\rm s} \approx 10^{35}$ erg s^{-1} requires a heating rate $\dot{q}_b > 3 \times 10^{19}$ erg s^{-1} cm^{-3} at shallow depths $z \lesssim 300$ m.

Two possible mechanisms for converting magnetic energy to heat are mechanical dissipation in the failing crust and ohmic heating. Both obey strong upper limits (Beloborodov & Li 2016). In particular, mechanical heating can only occur in the solid phase below the melted ocean, and its rate cannot exceed $\dot{q}_{\rm max} \sim 0.1\mu\dot{s}$, where $\mu \sim 10^{28}\rho_{12}$ erg cm^{-3} is the shear modulus of the lattice and $\dot{s}$ is the strain rate of the deformation. This leads to an upper limit on the persistent surface luminosity, which falls short of 10^{35} erg s^{-1}.

The rate of ohmic heating $\dot{q}_{\rm h} = j^2/\sigma$ is also limited, because of the high electric conductivity of the crustal material: $\sigma \sim 10^{22}$ s^{-1} in the relevant range of temperatures and densities in the upper crust (Potekhin et al. 2015b). The timescale for dissipating electric currents that sustain variations δB on a scale ℓ is $t_{\rm ohm} \sim 4\pi\sigma\ell^2/c^2 \sim 4 \times 10^4\,\sigma_{22}\,\ell_{\rm km}^2$ years. Ohmic dissipation could provide the required heating if two demanding conditions are satisfied: (*a*) $t_{\rm ohm}$ is sufficiently short, comparable with the magnetar age of 1–10 kyr, which requires a small scale of the field variations $\ell \sim 3 \times 10^4$ cm, and (*b*) the field variations on this scale must be huge, $\delta B \sim 10^{16}$ G, to provide $\dot{q}_b \sim (\delta B)^2/8\pi t_{\rm ohm} > 3 \times 10^{19}$ erg s^{-1} cm^{-3}.

It was proposed that ohmic and mechanical heating are boosted by Hall drift, which can transport magnetic energy to the shallow layers (Jones 1988) and develop large current densities (Goldreich & Reisenegger 1992). Heating of the crust reduces its conductivity, leading to the coupled evolution of temperature and magnetic field. This magnetothermal evolution was studied numerically (e.g., Pons et al. 2009, Viganò et al. 2013), showing inhomogeneous heating of the stellar surface on timescales comparable with the magnetar ages. The results suggest that the magnetothermal evolution of the crust may explain the observed properties of a broader class of neutron stars, not only magnetars.

For simplicity, the simulations assumed that the crust is static, and this assumption needs to be relaxed in more realistic models. Hall drift in the upper crust induces magnetic stresses exceeding the maximum elastic stress $\sigma_{\rm max} \sim 0.1\mu$, and the crust must flow, relieving the stress. This leads to an upper limit on Hall-driven dissipation, rendering it hardly capable of sustaining the surface luminosity of classical persistent magnetars (Beloborodov & Li 2016). The full magnetothermoplastic evolution has been simulated in a one-dimensional model by Li et al. (2016). It showed intermittent heating through avalanches developing due to the excitation of short Hall waves in the avalanche, which may explain the activity of transient magnetars.

5.2.3. Transient heating and flare afterglow. Lyubarsky et al. (2002) explored how a sudden deposition of heat in the crust could power the afterglow of the 1998 GF from SGR 1900+14. They found that heating would need to be approximately uniform throughout the upper crust, which implies enormous heat per unit mass in the surface layers $z < 100$ m. It is, however, unclear how magnetic energy could be suddenly dissipated in the shallow layers, which should

behave as a liquid ideal conductor during the flare. An additional complication is that the afterglow spectrum was nonthermal (Woods et al. 2001), suggesting magnetospheric origin. Nevertheless, the phenomenological picture of sudden crustal heating was applied to several transient magnetars, using detailed time-dependent simulations of heat conduction (e.g., Rea et al. 2013, Scholz et al. 2014). The model was found capable of reproducing the observed light curves of some transient magnetars, except the cases where the emission area was observed to shrink with time. A mechanism explaining this shrinking is discussed in Section 5.4.2.

A concrete mechanism for sudden crustal heating by a magnetospheric flare was recently described by Li & Beloborodov (2015). They showed that Alfvén waves generated by the flare are quickly absorbed by the star and damped into plastic heat in the solid crust immediately below the melted ocean. A fraction of the deposited heat is eventually conducted to the stellar surface, contributing to the surface afterglow months to years after the flare.

5.2.4. Surface spectrum. The spectrum of thermal radiation emerging from the hot magnetar deviates from a Planck spectrum because of radiative transfer effects, which are sensitive to the magnetic field [see Potekhin et al. (2015a) for a review]. An interesting potential spectral feature is the ion cyclotron line at energy $\hbar ZeB/Am_pc \approx 0.63\,(Z/A)B_{14}$ keV, where A and Z are the ion mass and charge numbers, respectively.

The first detailed simulations of magnetar spectra assumed a fully ionized hydrogen atmosphere (Ho & Lai 2001, Özel 2001, Zane et al. 2001); calculations have also been performed for a broader class of models. Instead of forming a low-density atmosphere, the surface may condense into a Coulomb liquid (Ruderman 1971, Medin & Lai 2006) with a high density $\rho \sim 10^5 AZ^{-3/5}B_{14}^{6/5}$ g cm^{-3}. In this case, the emerging spectrum depends on the reflectivity of the liquid surface (Turolla et al. 2004). It is also possible that the liquid is covered by a thin low-density atmosphere (Suleimanov et al. 2009).

Magnetar fields exceed the characteristic field $B_Q = m_e^2c^3/\hbar e \approx 4.4 \times 10^{13}$ G defined by $\hbar\omega_B = m_ec^2$, where $\omega_B = eB/m_ec$. As a result, the photon normal modes are significantly impacted by the quantum electrodynamic device effect of vacuum polarization as well as plasma polarization. Vacuum polarization dominates at densities $\rho \ll \rho_V \sim 1\,B_{14}^2(\hbar\omega/1\text{keV})^2$ g cm^{-3} and defines two linearly polarized normal modes: the ordinary or O-mode (polarized in the **k**-**B** plane, where **k** is the photon wave vector) and the extraordinary or X-mode (polarized perpendicular to the **k**-**B** plane). At densities $\rho \gg \rho_V$ the plasma polarization dominates, which also gives O- and X-modes with highly elliptical polarizations. As photons pass through the layer with $\rho = \rho_V$, the polarization ellipse rotates by 90°, effectively switching the modes $O \leftrightarrow X$ (Lai & Ho 2003), and the photon begins to see a different opacity. This effect tends to deplete the spectrum at high energies and also weakens the cyclotron absorption line.

In principle, the surface spectrum contains information on the surface magnetic field; however, in practice extracting this information is extremely difficult. The cyclotron line is hard to detect when its position is smeared out; this is due to variations in the surface magnetic field. Besides **B**, the surface spectrum depends on the chemical composition and possible condensation, and disentangling all the effects is a challenging task. Attempts to infer the surface **B** from the observed 1–10-keV spectrum (e.g., Güver et al. 2011) are further complicated by the superimposed magnetospheric emission.

The inhomogeneity of temperature and magnetic field on the stellar surface leads to flux pulsations with the magnetar spin period, which are influenced by the anisotropy of surface radiation and gravitational light bending. The surface radiation has a component beamed along the local **B** and a broader fan component peaking perpendicular to **B** (Zavlin et al. 1995). The observed pulse profiles are also strongly influenced by photon scattering in the magnetosphere.

5.2.5. Polarization. Thermal radiation diffusing toward the magnetar surface is dominated by the X-mode photons, which have longer free paths and hence escape from deeper and hotter atmospheric layers. This radiation is linearly polarized with the electric field perpendicular to the **k**-**B** plane. Radiation emerging from a condensed surface is also linearly polarized; polarization of the radiation emitted by gaseous and condensed surfaces is discussed in detail by Gonzalez Caniulef et al. (2016).

Polarization measured by a distant observer is influenced by two factors. (*a*) The observer receives surface radiation from regions with different magnetic fields, which implies some averaging of the polarization. (*b*) As the photons propagate through the magnetosphere, they adiabatically track the local normal mode defined by the local **B**: The polarization vector of the X-mode shifts so that it stays perpendicular to the **k**-**B** plane. This tracking ends, and the polarization angle freezes when the photon reaches the adiabatic radius $r_{\rm ad} \sim 80R\, B_{\rm s,14}^{2/5}(\hbar\omega/1\ {\rm keV})^{1/5}$, where $B_{\rm s}$ is the surface magnetic field (Heyl et al. 2003). Therefore, effectively the observed polarization angle is controlled by the direction of **B** at $r_{\rm ad}$ rather than at the stellar surface.

5.3. Flares

Magnetar flares and bursts emit hard X-rays and hence must be produced outside the neutron star. An internal trigger scenario assumes that the flares are triggered by an instability that leads to sudden ejection of magnetic energy from the stellar core to the magnetosphere. The trigger could be an MHD instability in the liquid core or a sudden failure of the solid crust in response to a slow buildup of magnetic stresses at the crust–core boundary (Thompson & Duncan 1995, 2001). Excitation of core motions with displacement ξ carries energy up to $\sim E_{\rm mag}(\xi/R)^2$, where $E_{\rm mag} \sim 10^{48}$ ergs is the putative magnetic energy of the core. A displacement $\xi \sim R$ would strongly deform the magnetosphere and trigger a GF; however, it implies a huge energy budget for the event, comparable with the entire $E_{\rm mag}$. A smaller ξ could provide sufficient energy for a GF; however, $\xi \ll R$ makes energy transfer to the magnetosphere inefficient (Link 2014).

An alternative external trigger scenario assumes a gradual deformation of the magnetosphere and the buildup of the free magnetic energy followed by its sudden release, similar to solar flares (Lyutikov 2003, Gill & Heyl 2010, Parfrey et al. 2013). This scenario requires only that the crustal motions pump an external twist faster than the magnetosphere damps it. This condition can be satisfied by thermoplastic crustal motions.

5.3.1. Magnetospheric instability. The magnetosphere twisted by surface shear motions becomes nonpotential, $\nabla \times \mathbf{B} \neq 0$, and threaded by electric currents $\mathbf{j} = (c/4\pi)\nabla \times \mathbf{B}$. The magnetic energy still dominates over the plasma energy (including its rest mass), and in the absence of strong ohmic dissipation the magnetosphere remains nearly force free, $\mathbf{j} \times \mathbf{B} \approx 0$. On a microscopic level, this condition corresponds to particles being kept in the ground Landau state in the strong magnetic field, so that charges can only flow along **B**.

Strongly deformed magnetospheres are prone to global instabilities, as shown by the analysis of twisted magnetic equilibria (e.g., Uzdensky 2002). An equilibrium magnetosphere obeys the equation $\nabla \times (\nabla \times \mathbf{B}) = 0$. The same equation describes the force-free solar corona, and the first models of static magnetar magnetospheres (Thompson et al. 2002) followed the self-similar solutions of Wolfson (1995). More realistic configurations are obtained by numerical simulations of the magnetosphere responding to surface shear (Parfrey et al. 2013). As the surface shearing continues, the twist angle ψ grows until it reaches a critical value at which the magnetosphere becomes unstable. Then it suddenly releases a significant fraction of the stored twist energy and produces a powerful flare. The flare involves a current sheet formation, its tearing instability and

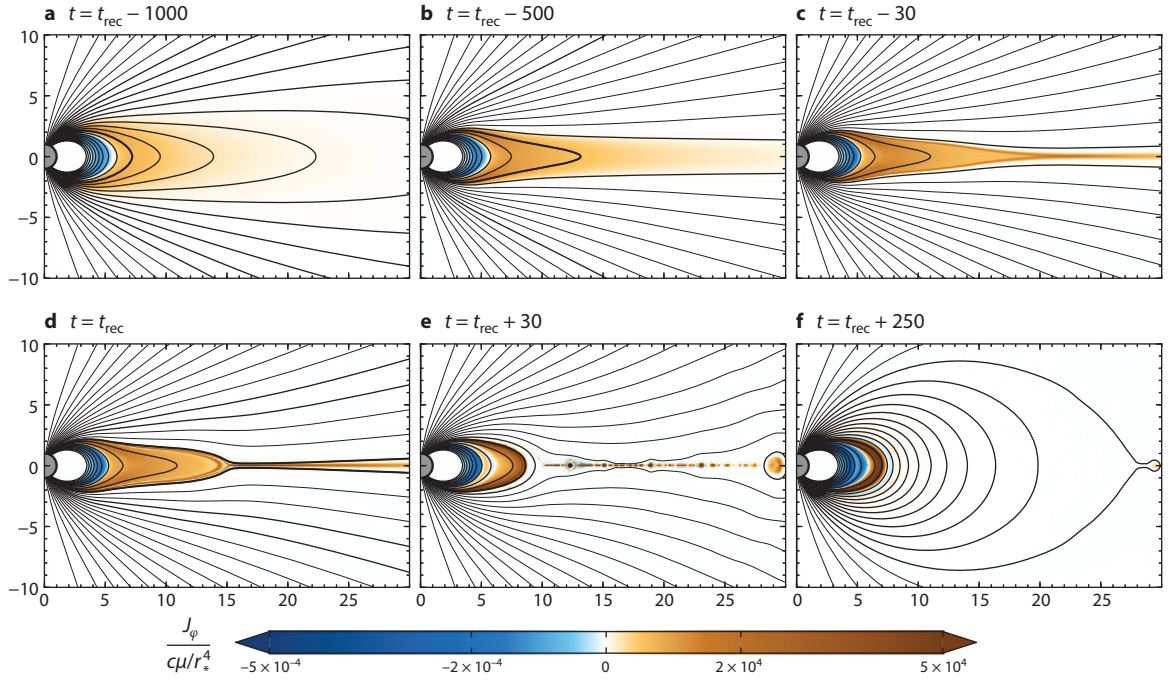

Figure 7

Formation of the current sheet in an over-twisted magnetosphere. Reconnection begins at t_{rec} (panel *d*). Color shows toroidal current density; lines are the poloidal magnetic field lines. One field line is highlighted in heavy black; it first opens and then closes again. Time is indicated in units of the light crossing time of the star. Adapted from Parfrey et al. (2013) with permission.

ejection of plasmoids, which resembles coronal mass ejections from the Sun (Mikic & Linker 1994). The flare development in axisymmetric geometry is shown in **Figure 7**. Future simulations can significantly advance this picture by relaxing axisymmetry and demonstrating the development of current sheets near the null points of more general magnetic configurations.

Current sheets spontaneously forming in over-twisted magnetospheres are fated to fast reconnection and energy dissipation. This process may naturally explain the fast onset of GFs, as the dynamical timescale of the magnetosphere is $\delta t \sim R/c < 1$ ms. However, tension exists between the observed duration of the main peak, $t_{peak} \sim 0.3$–0.5 s, and the theoretical duration of the reconnection event $\sim 10^2 R/c \sim 10^{-2}$ s (Uzdensky 2011).

5.3.2. Fast dissipation and radiation. The main spike of a GF releases $\sim 10^{44}$–10^{46} ergs, which implies a huge energy density near the star. It is consistent with dissipation of ultrastrong fields, releasing energy density up to $B^2/8\pi \approx 4 \times 10^{26} B_{14}^2$ erg cm^{-3}. The energy is immediately thermalized at a temperature $kT \gtrsim m_e c^2$, creating a dense population of $e^{\pm}$ pairs and making the region highly collisional and opaque. In addition to sudden heating, reconnection generates strong Alfvén waves, which are ducted along the magnetic field lines and trapped in the closed magnetosphere. Part of the wave energy may cascade to small scales and dissipate (Thompson & Blaes 1998), and part is damped in the star (Li & Beloborodov 2015).

The initial short spike of the GF must be emitted by a relativistic outflow that traps radiation near the star, advects it, and then releases it at a large radius $r > 10^{10}$ cm (Thompson & Duncan

1995). This process resembles what happens in a cosmological GRB (Mészáros 2002). A high Lorentz factor of the outflow Γ helps the radiation to escape, because the scattering optical depth is reduced as Γ^{-3}, and the photon–photon reaction $\gamma + \gamma \rightarrow e^+e^-$ is suppressed because of beaming of radiation within angle $\sim\Gamma^{-1}$.

After the initial spike, the temporarily opened field lines must close back to the star and trap a cloud of hot plasma ("fireball"), which produces the pulsating tail of the flare (Thompson & Duncan 1995). The fireball is confined if its energy E_0 is a fraction of $R^3B^2/8\pi \sim 10^{45}B_{14}^2$ ergs, so the field $B \gtrsim 10^{14}$ G is required by the observed energy radiated in the pulsating tail $E_0 \sim 10^{44}$ ergs. The trapped heat is gradually radiated away and the fireball gradually "evaporates," layer by layer. In the simplest model, the remaining heat $E(t)$ is proportional to the fireball volume while the luminosity $L = -\mathrm{d}E/\mathrm{d}t$ is proportional to the fireball surface area A. It implies $L \propto E^a$, where a may be between 2/3 (sphere) and 0 (slab), and gives $L(t) = L_0(1 - t/t_{\rm evap})^\chi$ with $0 < \chi = a/(1-a) < 2$ (Thompson & Duncan 2001). This relation fits the observed envelope of the pulsating tail after $\sim$40 s with $t_{\rm evap} \approx 6$ min and large $\chi = 3$, possibly indicating inhomogeneous structure of the fireball (Feroci et al. 2001). Further constraints on the model are provided by detailed calculations of neutrino losses (Gvozdev et al. 2011).

The emission observed during the first 40 s of the flare (and after its main peak) requires an additional source, which is brighter, less modulated by rotation, and also harder. It was interpreted as emission from a heated corona surrounding the fireball (Thompson & Duncan 2001). The emission observed after 40 s does not require additional heating and is dominated by the evaporating fireball. Its effective surface temperature $kT_{\rm s} \sim 15\,L_{42}^{1/4}A_{13}^{-1/4}$ keV is smaller than the temperature inside the fireball by a factor of $\sim 10^{-2}$. The mean photon energy in a blackbody spectrum, $\hbar\omega \sim 3kT_{\rm s}$, would be roughly consistent with the characteristic energy of observed hard X-rays; however, the radiation spectrum is not Planckian. The spectrum must be shaped by radiative transfer in the fireball, and a key feature of this transfer problem is the presence of two polarization states with drastically different free paths: the O- and X-modes. Scattering of the X-mode is suppressed by the factor of $\sim(\omega/\omega_B)^2 \sim 10^{-4}(\hbar\omega/10\ \mathrm{keV})^2 B_{14}^{-2}$. Therefore, the X-mode photons dominate the energy transport and the emerging luminosity; they escape from large Thomson optical depths where the O-mode photons are still trapped. Because the E-mode cross section scales as ω^2, photons of different energies $\hbar\omega$ escape from different depths, leading to a flat spectrum at $\hbar\omega \lesssim kT$ (Lyubarsky 2002). At high energies $\hbar\omega > kT$, the E-mode photons can split into O-mode photons in the ultrastrong magnetic field (Adler 1971). The resulting theoretical spectrum of escaping radiation is far from Planckian and resembles the observed broad spectrum. The amplitude of observed pulsations is likely affected by the scattering of fireball radiation in a continuing outflow from the star (Thompson & Duncan 2001, van Putten et al. 2016).

Similar fast dissipation of magnetic energy must occur in less powerful bursts, which are much more frequent than the GFs. Ordinary bursts with luminosity $L \ll 10^{42}$ erg s^{-1} may not be capable of producing fireballs with thermalized radiation, which explains their different spectra. The burst spectra are harder to model as they are more sensitive to the uncertainties in the dissipation mechanism, and detailed models have yet to be developed.

5.3.3. Quasi-periodic oscillations. The QPOs observed in GFs (Section 3.2.4) were interpreted as shear oscillations of the magnetar crust, which were studied by Duncan (1998). Simple QPO models assume that the crustal oscillations are decoupled from the liquid core (Piro 2005, Samuelsson & Andersson 2007). More realistic models allow for the crust coupling by the magnetic field to the continuum of Alfvén waves in the liquid core (Levin 2007). This creates significant uncertainties in the frequency spectrum of the global modes, as it depends on the magnetic

configuration in the star. However, some general features have been identified. The strongest oscillations are expected near the edges of the spectrum (van Hoven & Levin 2011). The oscillations experience phase mixing, and QPOs can be transient and delayed. The models may be reconciled with the observed range of QPO frequencies if neutrons are decoupled from the oscillations (van Hoven & Levin 2011, Gabler et al. 2013, Passamonti & Lander 2014), which is possible if the neutrons are superfluid. High-frequency oscillations, in particular the 625-Hz QPO in the 1998 GF, are most challenging to model.

The magnetosphere attached to the oscillating crust is periodically deformed (Gabler et al. 2014), which could lead to periodic changes in its luminosity. The models predict small amplitudes of surface oscillations, much smaller than the stellar radius, and it remains unclear how they generate the observed 10–20% modulation of the X-ray luminosity.

5.4. Gradual Energy Release in the Twisted Magnetosphere

The magnetosphere can remain twisted for years between the flares, explaining the magnetar activity described in Section 3. The presence of a magnetic twist $\nabla \times \mathbf{B} \neq 0$ implies long-lived electric currents, which are accompanied by some ohmic dissipation. The magnetosphere always tends to slowly untwist, and the released magnetic energy feeds its long-lived emission (Thompson et al. 2002, Beloborodov 2009).

5.4.1. Electric discharge. Magnetospheric electric currents can only flow along the magnetic field lines, and their ohmic dissipation occurs because of a small electric field $E_\parallel$ parallel to $\mathbf{B}$. The electric field has three functions: (*a*) It maintains the electric current $\mathbf{j} \parallel \mathbf{B}$ demanded by $\nabla \times \mathbf{B} \neq 0$, (*b*) it regulates the dissipation rate $E_\parallel j$ and the observed nonthermal luminosity, and (*c*) it determines the evolution of $\mathbf{B}$ in the untwisting magnetosphere according to the Maxwell–Faraday equation $\partial \mathbf{B}/\partial t = -c \nabla \times \mathbf{E}$.

The longitudinal voltage between the two footprints "1" and "2" of a magnetospheric field line, $\Phi_\parallel = -\int_1^2 E_\parallel \mathrm{d}l$, controls the ohmically released power $L \approx I\Phi_\parallel$, where $I < I_{\max} \sim c\mu/R^2$ is the net electric current circulating through the magnetosphere and μ is the magnetic dipole moment of the star. The observed nonthermal luminosities of magnetars typically require $\Phi_\parallel \sim 10^{10}$ V. The voltage was proposed to be regulated by $e^\pm$ discharge: When $\Phi_\parallel$ exceeds a threshold value, an exponential runaway of $e^\pm$ creation occurs until the pair plasma screens $E_\parallel$ (Beloborodov & Thompson 2007). As the plasma leaves the discharge region, $E_\parallel$ grows again and the discharge repeats, resembling continual lightning.

In a magnetar magnetosphere, the discharge is triggered when an electron accelerated to Lorentz factor γ begins to resonantly scatter X-rays streaming from the star. The X-ray photon is blueshifted in the electron rest frame by the factor of $\sim\gamma$, and resonant scattering occurs when the blueshifted photon frequency matches the cyclotron frequency $\omega_B = eB/m_e c$. In the ultrastrong field near the magnetar this typically requires $\gamma \gtrsim 10^3$. The scattered photon has a high energy $\sim\gamma^2$ keV and quickly converts to $e^\pm$ in the strong magnetic field. This process gives the threshold voltage $\Phi_\parallel \sim 10^9$–10^{10} V. The discharge can be modeled ab initio using the particle-in-cell (PIC) method that follows plasma particles individually in their collective electromagnetic field. First axisymmetric PIC simulations of twisted magnetospheres have been performed recently (Chen & Beloborodov 2016).

5.4.2. Resistive untwisting and shrinking hot spots. The resistive evolution of twisted magnetospheres has only been studied thus far in axisymmetric geometry. In this case the magnetosphere may be described as a foliation of axisymmetric flux surfaces labeled by magnetic flux function f,

and the twist of a magnetospheric field line $\psi(f)$ is the difference between the azimuthal angles of its footpoints on the star, $\psi = \phi_2 - \phi_1$. The twist evolution is governed by the electrodynamic equation obtained from $\partial \mathbf{B}/\partial t = -c \nabla \times \mathbf{E}$,

$$\frac{\partial \psi}{\partial t} = 2\pi c \frac{\partial \Phi_\parallel}{\partial f} + \omega(f, t), \tag{1}$$

where $\omega = \dot{\phi}_2 - \dot{\phi}_1$ is the applied shear rate at the stellar surface (Beloborodov 2009). When the fast crustal motions stop, so that $\omega \ll 2\pi c\, \partial \Phi_\parallel / \partial f$, the untwisting phase begins.

Two distinct regions evolve in an untwisting magnetosphere: a "cavity" with $j = 0$ and a "j-bundle" where the currents flow. The cavity comprises field lines that close near the star and has a sharp boundary along a flux surface $f_\star$. The process of resistive untwisting is the slow expansion of the boundary $f_\star$, which erases the electric currents in the j-bundle on a timescale $t_{\rm ohm} \lesssim \mu/c\, R\Phi_\parallel$. As a result, the magnetospheric currents have the longest lifetime on magnetic field lines with large apex radii $R_{\rm max} \gg R$; i.e., the magnetar activity tends to be confined to field lines extending far from the star.

This untwisting behavior implies a special observational feature: a slowly shrinking hot spot on the magnetar surface. The footprint of the j-bundle is expected to be hotter than the rest of the stellar surface, because it is bombarded by relativistic particles from the $e^\pm$ discharge. As the j-bundle slowly shrinks so does its footprint. The theoretically expected relation between the spot area A and luminosity L is given by $L \sim 1.3 \times 10^{33} K A_{11}^2$ erg s^{-1}, where $K = B_{14}\Phi_{\parallel 9}\psi$. Such shrinking hot spots have been observed in seven transient magnetars [see Beloborodov & Li (2016) for a compilation of data]. The spot area and luminosity decrease with time, and the observed slope of the A–L relation (controlled by the behavior of $\Phi_\parallel$) varies between 1 and 2. The typical timescale of this evolution, months to years, is also consistent with theoretical expectations.

Transient magnetars also show different behavior, which is inconsistent with the simple model of untwisting magnetosphere attached to a static crust. For instance, 1E 1547–5407 displays complicated activity (Kuiper et al. 2012a), possibly due to repeated twist injection, which prevents a clean, long twist decay. In addition, a different emission component may result from cooling of a suddenly heated crust, as discussed in Section 5.2.

5.4.3. Nonthermal X-rays. The dissipated twist energy is given to the $e^\pm$ plasma in the j-bundle, which can radiate it away in two ways: The particles can hit the stellar surface or pass their energy to the ambient X-rays streaming from the star, mainly through resonant Compton scattering (Thompson et al. 2002, Baring & Harding 2007).

Scattering of a keV photon by a particle with Lorentz factor γ boosts the photon energy by a factor of $\sim\gamma^2$. Early work (Thompson et al. 2002) proposed that the magnetosphere is filled with mildly relativistic electrons that scatter the thermal surface radiation and produce a soft power-law tail in the X-ray spectrum. The resonance scattering condition implies that mildly relativistic Comptonization can occur where $B \sim 10^{11}$ G, which corresponds to $\hbar e B/m_e c \sim 1$ keV; this region is typically at radii $r \sim 10R$. Detailed Comptonization models with ad hoc particle distributions were developed (Lyutikov & Gavriil 2006, Fernández & Thompson 2007, Nobili et al. 2008) and found capable of reproducing the observed 1–10-keV spectra. A simplified resonant Comptonization model was implemented under `XSPEC` and used to fit the X-ray spectra of magnetars below 10 keV (Rea et al. 2008, Zane et al. 2009).

Recent work attempted a self-consistent calculation of the particle motion in the j-bundle (2013a,b), which led to the picture shown in **Figure 8**. Pairs must be created with high Lorentz factors γ, and their subsequent motion is influenced by radiative losses caused by resonant scattering. The upscattered photons have high energies and convert to $e^\pm$ pairs in the region of

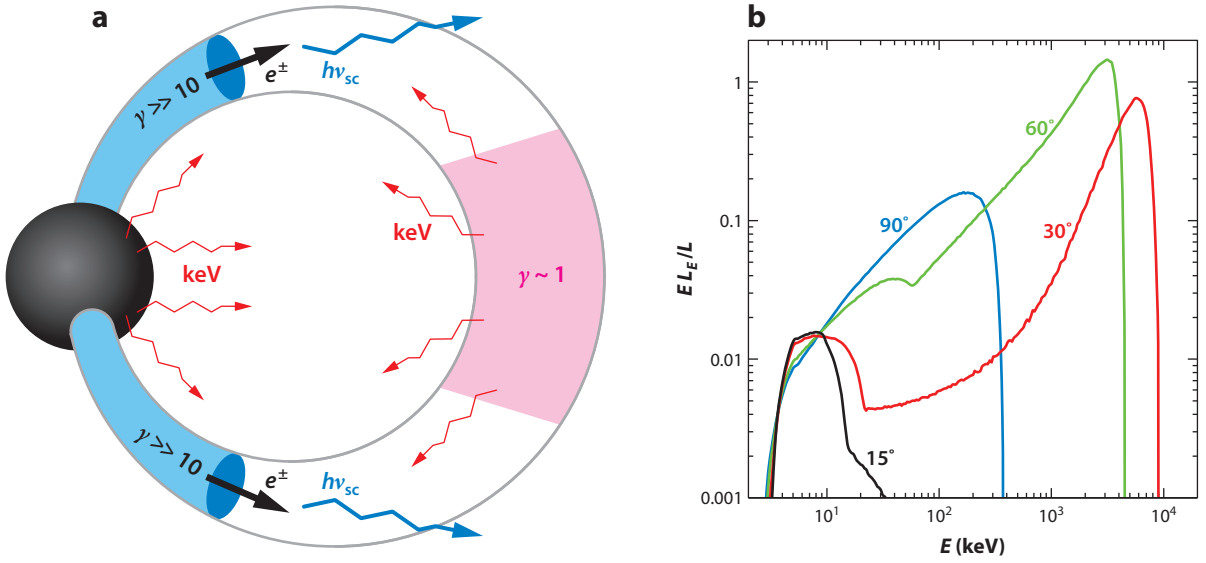

Figure 8

(*a*) A magnetic loop in the j-bundle. Relativistic particles are assumed to be injected near the star (*black sphere*), and a large $e^{\pm}$ multiplicity $\mathcal{M} \sim 100$ develops in the adiabatic zone $B > 10^{13}$ G (*blue shading*). The outer part of the loop is in the radiative zone; here the resonantly scattered photons of energy $h\nu_{sc} \sim 1\, B_{13}^2$ MeV escape and form the observed hard X-ray spectrum. The outflow decelerates and eventually annihilates at the top of the loop (*pink shading*); here it becomes opaque to the thermal keV photons flowing from the star. Photons reflected from the pink region have the best chance to be scattered by the relativistic outflow in the lower parts of the loop and control its deceleration. The footprint of the j-bundle is heated by the relativistic backflow from the discharge region; in an axisymmetric model it forms a hot ring on the stellar surface. (*b*) Radiation spectrum from the j-bundle viewed at four different angles with respect to the magnetic dipole axis. Adapted from Beloborodov (2013a) with permission.

$B > 10^{13}$ G. As a result, energy radiated near the star is processed into an outflow (fountain) of copious pairs with a standard profile of Lorentz factor $\gamma \approx 100(B/B_Q)$. The outflow radiates away its kinetic energy in the outer zone $B \lesssim 10^{13}$ G and comes to the top of the magnetic loop with $\gamma \sim 1$. Mildly relativistic Comptonization may occur in this outer region and influence the X-ray spectrum below 10 keV. However, most of the nonthermal luminosity is radiated above 10 keV in the lower parts of the loop, where the outflow has $\gamma \gg 1$.

Regardless of the details of the electric discharge near the star, the $e^{\pm}$ fountain emits a power-law spectrum $\mathrm{d}L/\mathrm{d}\ln E \propto E^{1/2}$. It naturally produces a distinct hard component in magnetar spectra, which peaks and cuts off in the MeV band. However, the $E^{1/2}$ power law is predicted only for spectra averaged over viewing angles. The emission is beamed along the magnetic field lines within angle $\sim\gamma^{-1} \sim 0.1\, B_{13}^{-1}$, and the overall angular distribution is determined by the field-line curvature. The field may be approximated as dipolar in the radiative zone $B \lesssim 10^{13}$ G, which is relatively far from the star. In this approximation, the predicted spectrum varies with the viewing angle as shown in **Figure 8**.

This model provided good fits to the phase-resolved hard X-ray spectra of magnetars (Hascoët et al. 2014, Vogel et al. 2014, An et al. 2015). The main unknown geometric parameters are the angle between the magnetic dipole axis and the rotation axis, $\alpha_{\rm mag}$, and the angle between the line of sight and the rotation axis, $\beta_{\rm obs}$. Remarkably, only a small region in the parameter space provided a good fit, which allows one to estimate $\alpha_{\rm mag}$ and $\beta_{\rm obs}$. The results suggest that the magnetic dipole axis in magnetars is slightly misaligned with the rotation axis.

The polarization of radiation upscattered in the magnetosphere was discussed by Fernández & Davis (2011) and Beloborodov (2013a). After resonant scattering the photon "forgets" its initial polarization; it becomes X-mode with 75% probability and O-mode with 25% probability. The escaping radiation should be dominated by the X-mode, except at energies approaching 1 MeV, where photon splitting occurs, $X \rightarrow O + O$ (Adler 1971). One may observe the O-mode polarization if the daughter photons from splitting do not scatter on the way out from the magnetosphere. Future measurements of X-ray polarization can provide powerful diagnostic tools, taking advantage of magnetar rotation (which gives a periodically changing viewing angle) and combining with the phase-resolved spectra.

A few other ideas were proposed for the origin of the hot plasma capable of emitting hard X-rays. Heyl & Hernquist (2005) discussed the possibility of shock formation by waves traveling in the magnetosphere. Thompson & Beloborodov (2005) proposed that a dense transition layer with $kT \sim 100$ keV forms between the magnetosphere and the stellar surface and radiates bremsstrahlung photons. This model does not, however, explain the variations of the hard X-ray spectrum with the rotational phase and why the emission at different energies peaks at different phases.

5.4.4. Low-frequency emission. In ordinary radio pulsars, radio emission is believed to come from the open field lines that connect the star to its light cylinder—this part of the magnetosphere is persistently active (twisted) and carries electric current $I_{\rm open} \sim \mu\Omega^2/2c$. The maximum voltage induced by stellar rotation on the open field lines is $\Phi_0 \approx \mu\Omega^2/c^2$ (Ruderman & Sutherland 1975). For typical magnetar parameters, $\mu \gtrsim 10^{32}$ G cm^3 and $\Omega \sim 1$ rad^{-1}, one finds $e\Phi_0/m_e c^2 \sim 10^8$, which is more than sufficient to sustain pair creation.

However, magnetar radio emission from the pair plasma in the open bundle may be undetectable for two reasons. (*a*) Pair discharge can limit the voltage to a much lower value $\Phi_\parallel \ll \Phi_0$; then the power dissipated in the open bundle is small: $\Phi_\parallel I_{\rm open} \sim 10^{29}(\Phi_\parallel/10^{10}{\rm V})$ erg s^{-1}. With a reasonable radiative efficiency this implies a low radio luminosity, well below $L_{\rm radio} \sim 10^{30}$ erg s^{-1} observed in XTE J1810–197 (Camilo et al. 2006). (*b*) The radio beam from the open bundle may be narrow and miss our line of sight.

The fact that radio pulsations are associated with outbursts (Section 3.3) suggests a connection with a magnetospheric twist. A scenario with strong dissipation on open field lines, $\Phi_\parallel I_{\rm open}$, enhanced by the twist in the closed magnetosphere (Thompson 2008), is problematic—this corresponds to $\partial\Phi_\parallel/\partial f < 0$ in Equation 1, and the twist around the open bundle should be quickly erased. Radio emission can be produced by the closed j-bundle itself. It is much thicker and more energetic than the open bundle and therefore capable of producing much brighter radio emission with a broad pulse. The untwisting magnetosphere in XTE J1810–197 had a j-bundle with magnetic flux $f_j \sim 3 \times 10^2 f_{\rm open}$ and carried electric current $I \sim 10^5 I_{\rm open}$. Then a reasonable efficiency of radio emission $L_{\rm radio}/\Phi_\parallel I \sim 10^{-3}$ is sufficient to explain the observed radio luminosity (Beloborodov 2009). Given the high plasma density in the j-bundle, $n \sim 10^{18}$–10^{20} cm^{-3}, the plasma frequency in the $e^\pm$ outflow may approach the IR or even optical band. Thus, plasma processes in the j-bundle might contribute to emission from radio to optical bands (Eichler et al. 2002).

5.5. Spin-Down Torque

The twisted magnetosphere of an active magnetar is somewhat inflated because of the additional pressure of the toroidal field $B_\phi^2/8\pi$. This inflation increases the open magnetic flux $f_{\rm open}$ that connects the star to its light cylinder and therefore increases the spin-down torque applied to the

star (Thompson et al. 2002). A strong increase in spin-down is expected for strong twists $\psi > 1$, which also produce a higher magnetospheric luminosity.

However, no strict general relation between the X-ray emission and spin-down is expected, particularly in nonaxisymmetric magnetospheres. The torque is sensitive to the behavior of the small flux bundle $f_{\rm open}$, a tiny fraction of the total magnetic flux of the star, $f_{\rm open}/f_{\rm total} \sim R/R_{\rm LC} \sim 10^{-4}$. The open flux is much smaller than $f_{\rm j}$ and may be outside the j-bundle. Therefore, the spin-down torque may react to changes in the magnetospheric twist with a delay or sometimes even anticorrelate with the X-ray emission, depending on the details of the magnetospheric configuration.

It was also proposed that the persistent high spin-down rate is caused by strong plasma loading of the magnetar wind (Harding et al. 1999, Tong et al. 2013a). This proposal posits that the true dipole component is much smaller than inferred from the standard spin-down formula $B \approx 3 \times 10^{19}(P\dot{P})^{1/2}$ G, and the magnetic energy required to feed the magnetar activity is stored in much stronger multipoles. A challenge for this scenario is that it needs a dense plasma outflow that would energetically dominate at the light cylinder and "comb out" the magnetic field lines, increasing the open magnetic flux and boosting the spin-down rate. It is unclear whether, e.g., seismic activity of the star would be able to drive such an outflow (Thompson et al. 2000).

Magnetospheric flares are expected to impact the magnetar spin-down. The existing flare simulations show that the magnetic flux connecting the star to its light cylinder $f_{\rm open}$ is dramatically increased during the flare, which is a result of strong inflation of the twisted field lines (Parfrey et al. 2013). The spin-down torque exerted on the star $\dot{J} \sim -f_{\rm open}^2/2\pi c P$ becomes enormous for a short time Δt comparable with $\Omega^{-1} = P/2\pi$ in the simulation, and produces a sudden increase of the rotation period $\Delta P > 0$—an antiglitch. When applied to the August 1998 GF in SGR 1900+14, the model gives $\Delta P/P \sim 10^{-4}$, which is consistent with the observed antiglitch (Woods et al. 1999). The predicted ΔP may vary in more realistic models where the flare is not axisymmetric and the light cylinder is far outside of the main flare region. This might explain the nondetection of an antiglitch ($\Delta P/P < 5 \times 10^{-6}$) in the exceptionally powerful GF of SGR 1806–20 on December 24, 2004, despite the observed ejection of a powerful outflow during the initial spike of the flare. Note also that the above picture does not work for antiglitches that are not associated with GFs, such as the one reported by Archibald et al. (2013).

6. CONCLUSIONS AND FUTURE WORK

The magnetar model has now been used to predict, naturally and uniquely, a wide variety of remarkable phenomena and behaviors in sources that once seemed highly anomalous. The now seamless chain of phenomenology from otherwise conventional radio pulsars through sources previously known for radically different behavior makes clear that these objects are one continuous family, with activity correlated with spin-inferred magnetic field strength. Recent advances in the physics of these objects, from the core through the crust and to the outer magnetosphere, hold significant promise. Below are issues we believe hold potential for important progress in the field in the near future, as well as remaining unsolved problems that are worthy of more thought.

FUTURE ISSUES

Why the transient magnetars are orders of magnitude fainter and significantly softer in X-rays than the persistent sources remains an important puzzle. Continued X-ray and multiwavelength follow-up of newly discovered magnetars, found using all-sky X-ray monitors sensitive to outbursts, will flesh out spin-property distributions and better constrain the Galactic population of transient magnetars and their outburst rates.

1. Future X-ray polarimetric observations of magnetars will test basic predictions of quantum electrodynamics and illuminate the geometry of the magnetic field for comparison with that inferred from modeling of phase-resolved hard X-ray spectra.
2. Monitoring of high-magnetic-field radio pulsars, particularly their behavior near glitch epochs and at rare times of magnetar-type activity, will help clarify the onset of instabilities with increasing spin-inferred magnetic field.
3. Detailed studies of magnetar wind nebulae and associations with TeV emission may be useful for calorimetric determinations of past magnetar activity.
4. Numerical simulations of ambipolar diffusion in the core and advanced magnetothermoplastic models of crust evolution may shed light on how magnetars become active and permit quantitative predictions for their transient and persistent activity.
5. First-principle simulations of twisted magnetospheres have now become possible using the plasma particle-in-cell method. This technique has recently been successfully applied to ordinary radio pulsars and can be applied to magnetars.
6. Three-dimensional simulations of relativistic reconnection in the magnetosphere can give more realistic models of bursts and giant flares.
7. The results of recent modeling of internal heating and post-flare QPOs provide strong constraints on magnetar interiors and can be used to infer basic properties such as superfluidity in the core and the strength of the internal magnetic field.
8. Modeling of the remarkable glitches and antiglitches observed in magnetars and their radiative signatures may become possible in the near future as part of detailed simulations of magnetar interiors that include superfluid neutrons.

DISCLOSURE STATEMENT

The authors are not aware of any affiliations, memberships, funding, or financial holdings that might be perceived as affecting the objectivity of this review.

ACKNOWLEDGMENTS

V.M.K. acknowledges funding from the Natural Sciences & Engineering Research Council of Canada, the Canada Research Chairs program, the Canadian Institute for Advanced Research, the Lorne Trottier Chair in Astrophysics & Cosmology, and Les Fonds de Recherche du Québec—Nature et Technologies. A.M.B. acknowledges NASA grant NNX13AI34G and a grant from the Simons Foundation (#446228).

LITERATURE CITED

Adler SL. 1971. *Ann. Phys.* 67:599–647
Akgün T, Reisenegger A, Mastrano A, Marchant P. 2013. *MNRAS* 433:2445–66
Alford JAJ, Halpern JP. 2016. *Ap. J.* 818:122
An H, Archibald RF, Hascoët R, et al. 2015. *Ap. J.* 807:93
An H, Kaspi VM, Archibald R, Cumming A. 2013. *Ap. J.* 763:82
An H, Kaspi VM, Beloborodov AM, et al. 2014. *Ap. J.* 790:60

An H, Kaspi VM, Tomsick JA, et al. 2012. *Ap. J.* 757:68
Anderson PW, Itoh N. 1975. *Nature* 256:25–27
Archibald AM, Kaspi VM, Livingstone MA, McLaughlin MA. 2008. *Ap. J.* 688:550–54
Archibald RF, Kaspi VM, Beardmore AP, Gehrels N, Kennea JA. 2015a. *Ap. J.* 810:67
Archibald RF, Kaspi VM, Ng CY, et al. 2013. *Nature* 497:591–93
Archibald RF, Kaspi VM, Ng CY, et al. 2015b. *Ap. J.* 800:33
Archibald RF, Kaspi VM, Tendulkar SP, Scholz P. 2016a. *Ap. J. Lett.* 829:L21
Archibald RF, Tendulkar SP, Scholz P, Kaspi VM. 2016b. *Astron. Telegr.* 9316
Arzoumanian Z, Chernoff DF, Cordes JM. 2002. *Ap. J.* 568:289–301
Baring MG, Harding AK. 2007. *Ap. Space Sci.* 308:109–18
Baykal A, Strohmayer T, Swank J, Alpar A, Stark MJ. 2000. *MNRAS* 319:205–8
Baykal A, Swank J. 1996. *Ap. J.* 460:470–77
Beloborodov AM. 2009. *Ap. J.* 703:1044–60
Beloborodov AM. 2013a. *Ap. J.* 762:13
Beloborodov AM. 2013b. *Ap. J.* 777:114
Beloborodov AM, Levin Y. 2014. *Ap. J. Lett.* 794:L24
Beloborodov AM, Li X. 2016. *Ap. J.* 833:261
Beloborodov AM, Thompson C. 2007. *Ap. J.* 657:967–93
Berger E. 2014. *Annu. Rev. Astron. Astrophys.* 52:43–105
Boggs SE, Zoglauer A, Bellm E, et al. 2007. *Ap. J.* 661:458–67
Bower GC, Deller A, Demorest P, et al. 2014. *Ap. J. Lett.* 780:L2
Braithwaite J. 2009. *MNRAS* 397:763–74
Brisken WF, Fruchter AS, Goss WM, Herrnstein RS, Thorsett SE. 2003. *Astron. J.* 126:3090–98
Burgay M, Possenti A, Kerr M, et al. 2016. *Astron. Telegr.* 9286
Camero-Arranz A, Rea N, Bucciantini N, et al. 2013. *MNRAS* 429:2493–99
Camilo F, Ransom SM, Halpern JP, et al. 2006. *Nature* 442:892–95
Camilo F, Ransom SM, Halpern JP, et al. 2016. *Ap. J.* 820:110
Camilo F, Ransom SM, Halpern JP, Reynolds J. 2007a. *Ap. J.* 666:L93–96
Camilo F, Ransom SM, Peñalver J, et al. 2007b. *Ap. J.* 669:561–69
Camilo F, Reynolds J, Johnston S, Halpern JP, Ransom SM. 2008. *Ap. J.* 679:681–86
Chakraborty M, Göğüş E, Şaşmaz Muş S, Kaneko Y. 2016. *Ap. J.* 819:153
Chen AY, Beloborodov AM. 2016. *Ap. J.* Submitted. arXiv:1610.10036
Chugunov AI, Horowitz CJ. 2010. *MNRAS* 407:L54–58
Cline TL, Desai UD, Teegarden BJ, et al. 1982. *Ap. J.* 255:L45–48
Colpi M, Geppert U, Page D. 2000. *Ap. J.* 529:L29–32
Cordes JM, Lazio TJW. 2001. *Ap. J.* 549:997–1010
D'Aì A, Evans PA, Burrows DN, et al. 2016. *MNRAS* 463:2394
Dall'Osso S, Israel GL, Stella L, Possenti A, Perozzi E. 2003. *Ap. J.* 599:485–97
De Luca A, Caraveo PA, Mereghetti S, Tiengo A, Bignami GF. 2006. *Science* 313:814–17
den Hartog PR, Kuiper L, Hermsen W. 2008a. *Astron. Astrophys.* 489:263–79
den Hartog PR, Kuiper L, Hermsen W, et al. 2008b. *Astron. Astrophys.* 489:245–61
Dhillon VS, Marsh TR, Hulleman F, et al. 2005. *MNRAS* 363:609–14
Dhillon VS, Marsh TR, Littlefair SP, et al. 2009. *MNRAS* 394:L112–16
Dhillon VS, Marsh TR, Littlefair SP, et al. 2011. *MNRAS* 416:L16–20
Dib R, Kaspi VM. 2014. *Ap. J.* 784:37
Dib R, Kaspi VM, Gavriil FP. 2008. *Ap. J.* 673:1044–61
Duncan RC. 1998. *Ap. J. Lett.* 498:L45–49
Duncan RC, Thompson C. 1992. *Ap. J.* 392:L9–13
Durant M, van Kerkwijk MH. 2006. *Ap. J.* 652:576–83
Eatough RP, Falcke H, Karuppusamy R, et al. 2013. *Nature* 501:391–94
Eichler D, Gedalin M, Lyubarsky Y. 2002. *Ap. J.* 578:L121–24
Enoto T, Nakazawa K, Makishima K, et al. 2010. *Ap. J. Lett.* 722:L162–67
Esposito P, Tiengo A, Rea N, et al. 2013. *MNRAS* 429:3123–32

Evans WD, Klebesadel RW, Laros JG, et al. 1980. *Ap. J.* 237:L7–9
Fahlman GG, Gregory PC. 1981. *Nature* 293:202–4
Faucher-Giguère CA, Kaspi VM. 2006. *Ap. J.* 643:332–55
Fenimore EE, Evans WD, Klebesadel RW, Laros JG, Terrell J. 1981. *Nature* 289:42
Fernández R, Davis SW. 2011. *Ap. J.* 730:131
Fernández R, Thompson C. 2007. *Ap. J.* 660:615–40
Feroci M, Hurley K, Duncan RC, Thompson C. 2001. *Ap. J.* 549:1021–38
Ferrario L, Wickramasinghe D. 2006. *MNRAS* 367:1323–28
Flowers EG, Ruderman M, Sutherland PG. 1976. *Ap. J.* 205:241
Frail DA, Kulkarni SR, Bloom JS. 1999. *Nature* 398:127–29
Gabler M, Cerdá-Durán P, Stergioulas N, Font JA, Müller E. 2013. *Phys. Rev. Lett.* 111:211102
Gabler M, Cerdá-Durán P, Stergioulas N, Font JA, Müller E. 2014. *MNRAS* 443:1416–24
Gaensler BM, Kouveliotou C, Gelfand JD, et al. 2005. *Nature* 434:1104–6
Gaensler BM, Slane PO. 2006. *Annu. Rev. Astron. Astrophys.* 44:17–47
Gavriil FP, Dib R, Kaspi VM. 2011. *Ap. J.* 736:138
Gavriil FP, Gonzalez ME, Gotthelf EV, et al. 2008. *Science* 319:1802–5
Gavriil FP, Kaspi VM, Woods PM. 2002. *Nature* 419:142–44
Gavriil FP, Kaspi VM, Woods PM. 2004. *Ap. J.* 607:959–69
Gelfand JD, Lyubarsky YE, Eichler D, et al. 2005. *Ap. J. Lett.* 634:L89–92
Gill R, Heyl JS. 2010. *MNRAS* 407:1926–32
Glampedakis K, Jones DI, Samuelsson L. 2011. *MNRAS* 413:2021–30
Goldreich P, Reisenegger A. 1992. *Ap. J.* 395:250–58
Gonzalez ME, Dib R, Kaspi VM, et al. 2010. *Ap. J.* 716:1345–55
Gonzalez Caniulef D, Zane S, Taverna R, et al. 2016. *MNRAS* 459:3585–95
Gotthelf EV, Halpern JP. 2007. *Ap. J.* 664:L35–38
Gotthelf EV, Halpern JP, Buxton M, Bailyn C. 2004. *Ap. J.* 605:368–77
Gotthelf EV, Vasisht G, Boylan-Kolchin M, Torii K. 2000. *Ap. J.* 542:L37–40
Göğüş E, Güver T, Özel F, Eichler D, Kouveliotou C. 2011a. *Ap. J.* 728:160
Göğüş E, Lin L, Kaneko Y, et al. 2016. *Ap. J. Lett.* 829:L25
Göğüş E, Kouveliotou C, Woods PM, et al. 2001. *Ap. J.* 558:228–36
Göğüş E, Woods PM, Kouveliotou C, et al. 1999. *Ap. J.* 526:L93–96
Göğüş E, Woods PM, Kouveliotou C, et al. 2000. *Ap. J.* 532:L121–24
Göğüş E, Woods PM, Kouveliotou C, et al. 2011b. *Ap. J.* 740:55
Götz D, Mereghetti S, Tiengo A, Esposito P. 2006. *Astron. Astrophys.* 449:L31–34
Gourgouliatos KN, Cumming A. 2014. *MNRAS* 438:1618–29
Gourgouliatos KN, Wood TS, Hollerbach R. 2016. *PNAS* 113:3944–49
Gregory PC, Fahlman GG. 1980. *Nature* 287:805–6
Güver T, Göğüş E, Özel F. 2011. *MNRAS* 418:2773–78
Gvozdev AA, Ognev IS, Osokina EV. 2011. *Astron. Lett.* 37:332–42
Halpern JP, Gotthelf EV. 2010. *Ap. J.* 709:436–46
Harding AK, Contopoulos I, Kazanas D. 1999. *Ap. J.* 525:L125–28
Hascoët R, Beloborodov AM, den Hartog PR. 2014. *Ap. J. Lett.* 786:L1
Helfand DJ. 1994. *MNRAS* 267:490
Heyl JS, Hernquist L. 2005. *Ap. J.* 618:463–73
Heyl JS, Shaviv NJ, Lloyd D. 2003. *MNRAS* 342:134
Ho WCG, Andersson N. 2017. *MNRAS* 464:65
Ho WCG, Lai D. 2001. *MNRAS* 327:1081–96
Horowitz CJ, Kadau K. 2009. *Phys. Rev. Lett.* 102:191102
Huppenkothen D, D'Angelo C, Watts AL, et al. 2014. *Ap. J.* 787:128
Huppenkothen D, Watts AL, Uttley P, et al. 2013. *Ap. J.* 768:87
Hurley K, Boggs SE, Smith DM, et al. 2005. *Nature* 434:1098–103
Hurley K, Cline T, Mazets E, et al. 1999. *Nature* 397:41–43
Hurley K, Rowlinson A, Bellm E, et al. 2010. *MNRAS* 403:342–52

Ibrahim AI, Markwardt CB, Swank JH, et al. 2004. *Ap. J.* 609:L21–24
Icdem B, Baykal A, Inam SC. 2012. *MNRAS* 419:3109–14
Israel G, Covino S, Mignani R, et al. 2005a. *Astron. Astrophys.* 438:L1–4
Israel GL, Belloni T, Stella L, et al. 2005b. *Ap. J. Lett.* 628:L53–56
Israel GL, Esposito P, Rea N, et al. 2010. *MNRAS* 408:1387–95
Israel GL, Mereghetti S, Stella L. 1994. *Ap. J.* 433:L25–28
Israel GL, Oosterbroek T, Angelini L, et al. 1999. *Astron. Astrophys.* 346:929–35
Jones PB. 1988. *MNRAS* 233:875–85
Jones PB. 2003. *Ap. J.* 595:342–45
Kaminker AD, Kaurov AA, Potekhin AY, Yakovlev DG. 2014. *MNRAS* 442:3484–94
Kargaltsev O, Kouveliotou C, Pavlov GG, et al. 2012. *Ap. J.* 748:26
Kaspi VM. 2010. *PNAS* 107:7147–52
Kaspi VM, Boydstun K. 2010. *Ap. J. Lett.* 710:L115–20
Kaspi VM, Chakrabarty D, Steinberger J. 1999. *Ap. J.* 525:L33–36
Kaspi VM, Gavriil FP. 2003. *Ap. J.* 596:L71–74
Kaspi VM, Gavriil FP, Woods PM, et al. 2003. *Ap. J.* 588:L93
Kaspi VM, Kramer M. 2015. In *Proc. 26th Solvay Conf. Phys. Astrophys. Cosmol., Brussels, Belgium*, Oct. 9–11, pp. 22–61. Singapore: World Sci. arXiv:1602.07738
Kaspi VM, Lackey JR, Chakrabarty D. 2000. *Ap. J.* 537:L31–34
Kaspi VM, McLaughlin MA. 2005. *Ap. J.* 618
Kennea JA, Burrows DN, Kouveliotou C, et al. 2013. *Ap. J. Lett.* 770:L24
Kennea JA, Lien AY, Marshall FE, et al. 2016. *Gamma-ray Coord. Netw. Circ.* 19735
Kern B, Martin C. 2002. *Nature* 415:527–29
Kouveliotou C, Dieters S, Strohmayer T, et al. 1998. *Nature* 393:235–37
Kouveliotou C, Norris JP, Cline TL, et al. 1987. *Ap. J. Lett.* 322:L21–25
Kouveliotou C, Strohmayer T, Hurley K, et al. 1999. *Ap. J.* 510:L115–18
Kuiper L, Hermsen W. 2009. *Astron. Astrophys.* 501:1031–46
Kuiper L, Hermsen W, den Hartog P, Collmar W. 2006. *Ap. J.* 645:556–75
Kuiper L, Hermsen W, den Hartog PR, Urama JO. 2012. *Ap. J.* 748:133
Kuiper L, Hermsen W, Mendez M. 2004. *Ap. J.* 613:1173–78
Kulkarni SR, Kaplan DL, Marshall HL, et al. 2003. *Ap. J.* 585:948–54
Kumar HS, Safi-Harb S. 2008. *Ap. J.* 678:L43–46
Lai D, Ho WC. 2003. *Phys. Rev. Lett.* 91:071101
Lander SK, Andersson N, Antonopoulou D, Watts AL. 2015. *MNRAS* 449:2047–58
Laros JG, Fenimore EE, Klebesadel RW, et al. 1987. *Ap. J. Lett.* 320:L111–15
Lazaridis K, Jessner A, Kramer M, et al. 2008. *MNRAS* 390:839–46
Lazarus P, Kaspi VM, Champion DJ, Hessels JWT, Dib R. 2012. *Ap. J.* 744:97
Lenters GT, Woods PM, Goupell JE, et al. 2003. *Ap. J.* 587:761–70
Levin L, Bailes M, Bates S, et al. 2010. *Ap. J. Lett.* 721:L33–37
Levin L, Bailes M, Bates SD, et al. 2012. *MNRAS* 422:2489–500
Levin Y. 2007. *MNRAS* 377:159–67
Levin Y, Lyutikov M. 2012. *MNRAS* 427:1574–79
Li X. 2007. *Ap. J.* 666:L81–84
Li X, Beloborodov AM. 2015. *Ap. J.* 815:25
Li X, Levin Y, Beloborodov AM. 2016. *Ap. J.* 833:189
Lin L, Göğüş E, Kaneko Y, Kouveliotou C. 2013. *Ap. J.* 778:105
Link B. 2014. *MNRAS* 441:2676–83
Link B, Epstein RI. 1996. *Ap. J.* 457:844
Livingstone MA, Kaspi VM, Gavriil FP. 2010. *Ap. J.* 710:1710–17
Livingstone MA, Ng CY, Kaspi VM, Gavriil FP, Gotthelf EV. 2011. *Ap. J.* 730:66
Lynch RS, Archibald RF, Kaspi VM, Scholz P. 2015. *Ap. J.* 806:266
Lyubarsky Y, Eichler D, Thompson C. 2002. *Ap. J.* 580:L69–72
Lyubarsky YE. 2002. *MNRAS* 332:199–204

Lyutikov M. 2003. *MNRAS* 339:623–32
Lyutikov M, Gavriil FP. 2006. *MNRAS* 368:690–706
Maron O, Kijak J, Kramer M, Wielebinski R. 2000. *Astron. Astrophys. Suppl.* 147:195–203
Marsden D, White NE. 2001. *Ap. J.* 551:L155–58
Martin J, Rea N, Torres DF, Papitto A. 2014. *MNRAS* 444:2910–24
Mazets EP, Golenetskii SV. 1981. *Ap. Space Sci.* 75:47–81
Mazets EP, Golenetskii SV, Gur'yan YA. 1979a. *Sov. Astron. Lett.* 5:343–44
Mazets EP, Golenetskii SV, Ilinskii VN, Apetkar RL, Guryan YA. 1979b. *Nature* 282:587–89
Medin Z, Lai D. 2006. *Phys. Rev. A* 74:062508
Mereghetti S, Götz D, Mirabel IF, Hurley K. 2005a. *Astron. Astrophys.* 433:L9–12
Mereghetti S, Götz D, von Kienlin A, et al. 2005b. *Ap. J. Lett.* 624:L105–8
Mereghetti S, Götz D, Weidenspointner G, et al. 2009. *Ap. J. Lett.* 696:L74–78
Mereghetti S, Pons JA, Melatos A. 2015. *Space Sci. Rev.* 191:315–38
Mereghetti S, Stella L. 1995. *Ap. J.* 442:L17–20
Mészáros P. 2002. *Annu. Rev. Astron. Astrophys.* 40:137–69
Mikic Z, Linker JA. 1994. *Ap. J.* 430:898–912
Mori K, Gotthelf EV, Zhang S, et al. 2013. *Ap. J. Lett.* 770:L23
Muş SŞ, Göğüş E, Kaneko Y, Chakraborty M, Aydn B. 2015. *Ap. J.* 807:42
Ng CY, Kaspi VM. 2011. In *Astrophysics of Neutron Stars 2010: A Conference in Honor of M. Ali Alpar*, ed. E Göğüş, T Belloni, Ü Ertan, 1379:70. Melville, NY: AIP
Ng CY, Kaspi VM, Dib R, Olausen SA, Scholz P, et al. 2011. *Ap. J.* 729:131
Nobili L, Turolla R, Zane S. 2008. *MNRAS* 386:1527–42
Ofek EO, Muno M, Quimby R, et al. 2008. *Ap. J.* 681:1464–69
Olausen SA, Kaspi VM. 2014. *Ap. J. Suppl. Ser.* 212:6
Olausen SA, Kaspi VM, Ng CY, et al. 2011. *Ap. J.* 742:4
Olausen SA, Zhu WW, Vogel JK, et al. 2013. *Ap. J.* 764:1
Özel F. 2001. *Ap. J.* 563:276–88
Paczyński B. 1992. *Acta Astron.* 42:145–53
Parfrey K, Beloborodov AM, Hui L. 2013. *Ap. J.* 774:92
Passamonti A, Lander SK. 2014. *MNRAS* 438:156–68
Pennucci TT, Possenti A, Esposito P, et al. 2015. *Ap. J.* 808:81
Perna R, Pons JA. 2011. *Ap. J. Lett.* 727:L51
Piro AL. 2005. *Ap. J. Lett.* 634:L153–56
Pons JA, Miralles JA, Geppert U. 2009. *Astron. Astrophys.* 496:207–16
Potekhin AY, De Luca A, Pons JA. 2015a. *Space Sci. Rev.* 191:171–206
Potekhin AY, Pons JA, Page D. 2015b. *Space Sci. Rev.* 191:239–91
Potekhin AY, Yakovlev DG, Chabrier G, Gnedin OY. 2003. *Ap. J.* 594:404–18
Rea N, Borghese A, Esposito P, et al. 2016. *Ap. J.* 828:L13
Rea N, Esposito P. 2011. *Ap. Space Sci.* 21:247
Rea N, Esposito P, Turolla R, et al. 2010. *Science* 330:944
Rea N, Israel GL, Esposito P, et al. 2012. *Ap. J.* 754:27
Rea N, Israel GL, Pons JA, et al. 2013. *Ap. J.* 770:65
Rea N, Israel GL, Turolla R, et al. 2009a. *MNRAS* 396:2419–32
Rea N, McLaughlin MA, Gaensler BM, et al. 2009b. *Ap. J.* 703:L41–45
Rea N, Testa V, Israel GL, et al. 2004. *Astron. Astrophys.* 425:L5–8
Rea N, Zane S, Turolla R, Lyutikov M, Götz D. 2008. *Ap. J.* 686:1245–60
Rodríguez Castillo GA, Israel GL, Tiengo A, et al. 2016. *MNRAS* 456:4145–55
Ruderman M. 1971. *Phys. Rev. Lett.* 27:1306–8
Ruderman MA, Sutherland PG. 1975. *Ap. J.* 196:51–72
Samuelsson L, Andersson N. 2007. *MNRAS* 374:256–68
Şaşmaz Muş S, Aydn B, Göğüş E. 2014. *MNRAS* 440:2916–21
Scholz P, Archibald RF, Kaspi VM, et al. 2014. *Ap. J.* 783:99
Scholz P, Kaspi VM. 2011. *Ap. J.* 739:94

Scholz P, Kaspi VM, Cumming A. 2014. *Ap. J.* 786:62
Seward FD, Charles PA, Smale AP. 1986. *Ap. J.* 305:814–16
Shannon RM, Johnston S. 2013. *MNRAS*
Spitler LG, Lee KJ, Eatough RP, et al. 2014. *Ap. J. Lett.* 780:L3
Spruit HC. 2008. In *40 Years of Pulsars: Millisecond Pulsars, Magnetars and More*, ed. C Bassa, Z Wang, A Cumming, VM Kaspi, *AIP Conf. Ser.* 983:391–98. Melville, NY: AIP
Stella L, Mereghetti S, Israel GL. 1996. *Mem. Soc. Astron. Ital.* 67:1053
Strohmayer TE, Watts AL. 2005. *Ap. J. Lett.* 632:L111–14
Suleimanov V, Potekhin AY, Werner K. 2009. *Astron. Astrophys.* 500:891–99
Tam CR, Gavriil FP, Dib R, et al. 2008. *Ap. J.* 677:503–14
Tam CR, Kaspi VM, van Kerkwijk MH, Durant M. 2004. *Ap. J.* 617:L53–56
Tendulkar SP, Cameron PB, Kulkarni SR. 2013. *Ap. J.* 772:31
Tendulkar SP, Hascöet R, Yang C, et al. 2015. *Ap. J.* 808:32
Tendulkar SP, Kaspi VM, Patel C. 2016. *Ap. J.* 827:59
Testa V, Rea N, Mignani RP, et al. 2008. *Astron. Astrophys.* 482:607–15
Thompson C. 2008. *Ap. J.* 688:499–526
Thompson C, Beloborodov AM. 2005. *Ap. J.* 634:565–69
Thompson C, Blaes O. 1998. *Phys. Rev. D* 57:3219–34
Thompson C, Duncan RC. 1995. *MNRAS* 275:255–300
Thompson C, Duncan RC. 1996. *Ap. J.* 473:322–42
Thompson C, Duncan RC. 2001. *Ap. J.* 561:980–1005
Thompson C, Duncan RC, Woods PM, et al. 2000. *Ap. J.* 543:340–50
Thompson C, Lyutikov M, Kulkarni SR. 2002. *Ap. J.* 574:332–55
Tiengo A, Esposito P, Mereghetti S, et al. 2009. *MNRAS* 399:L74–78
Tiengo A, Esposito P, Mereghetti S, et al. 2013. *Nature* 500:312–14
Tong H, Xu RX, Song LM, Qiao GJ. 2013a. *Ap. J.* 768:144
Tong H, Yuan JP, Liu ZY. 2013b. *Res. Astron. Astrophys.* 13:835–40
Torne P, Eatough RP, Karuppusamy R, et al. 2015. *MNRAS* 451:L50–54
Turolla R, Zane S, Drake JJ. 2004. *Ap. J.* 603:265–82
Turolla R, Zane S, Watts AL. 2015. *Rep. Progress Phys.* 78:116901
Uzdensky DA. 2002. *Ap. J.* 574:1011–20
Uzdensky DA. 2011. *Space Sci. Rev.* 160:45–71
van der Horst AJ, Kouveliotou C, Gorgone NM, et al. 2012. *Ap. J.* 749:122
van Hoven M, Levin Y. 2011. *MNRAS* 410:1036–51
van Paradijs J, Taam RE, van den Heuvel EPJ. 1995. *Astron. Astrophys.* 299:L41–44
van Putten T, Watts AL, Baring MG, Wijers RAMJ. 2016. *MNRAS* 461:877–91
Viganò D, Rea N, Pons JA, et al. 2013. *MNRAS* 434:123–41
Vink J, Kuiper L. 2006. *MNRAS* 370:L14–18
Vogel JK, Hascoët R, Kaspi VM, et al. 2014. *Ap. J.* 789:75
von Kienlin A, Gruber D, Kouveliotou C, et al. 2012. *Ap. J.* 755:150
Wang Z, Bassa C, Kaspi VM, et al. 2008. *Ap. J.* 679:1443–46
Wang Z, Chakrabarty D, Kaplan DL. 2006. *Nature* 440:772–75
Watts AL, Strohmayer TE. 2006. *Ap. J. Lett.* 637:L117–20
Wolfson R. 1995. *Ap. J.* 443:810–17
Woods PM, Kaspi VM, Thompson C, et al. 2004. *Ap. J.* 605:378–99
Woods PM, Kouveliotou C, Finger MH, et al. 2007. *Ap. J.* 654:470–86
Woods PM, Kouveliotou C, Gavriil FP, et al. 2005. *Ap. J.* 629:985–97
Woods PM, Kouveliotou C, Göğüş E, et al. 2001. *Ap. J.* 552:748–55
Woods PM, Kouveliotou C, van Paradijs J, et al. 1999. *Ap. J.* 524:L55–58
Woods PM, Thompson C. 2006. In *Compact Stellar X-ray Sources*, ed. WHG Lewin, M van der Klis. Cambridge, UK: Cambridge Univ. Press
Yakovlev DG, Pethick CJ. 2004. *Annu. Rev. Astron. Astrophys.* 42:169–210
Yakovlev DG, Shalybkov DA. 1990. *Sov. Astron. Lett.* 16:86

Younes G, Kouveliotou C, Kargaltsev O, et al. 2016. *Ap. J.* 824:138
Younes G, Kouveliotou C, Roberts O. 2016. *GCN* 19736
Yu M, Manchester RN, Hobbs G, et al. 2013. *MNRAS* 429:688–724
Zane S, Rea N, Turolla R, Nobili L. 2009. *MNRAS* 398:1403–13
Zane S, Turolla R, Stella L, Treves A. 2001. *Ap. J.* 560:384–89
Zavlin VE, Pavlov GG, Shibanov YA, Ventura J. 1995. *Astron. Astrophys.* 297:441
Zhu WW, Kaspi VM, McLaughlin MA, et al. 2011. *Ap. J.* 734:44

Contents

Annual Review of Astronomy and Astrophysics

Volume 55, 2017

Galaxies, Globular Clusters, and Dark Matter
Kenneth C. Freeman 1

Stellar Dynamics and Stellar Phenomena Near a Massive Black Hole
Tal Alexander 17

Theoretical Challenges in Galaxy Formation
Thorsten Naab and Jeremiah P. Ostriker 59

Observing Interstellar and Intergalactic Magnetic Fields
J.L. Han 111

Stellar Model Chromospheres and Spectroscopic Diagnostics
Jeffrey L. Linsky 159

Markov Chain Monte Carlo Methods for Bayesian Data Analysis in Astronomy
Sanjib Sharma 213

Magnetars
Victoria M. Kaspi and Andrei M. Beloborodov 261

Ultraluminous X-Ray Sources
Philip Kaaret, Hua Feng, and Timothy P. Roberts 303

Small-Scale Challenges to the ΛCDM Paradigm
James S. Bullock and Michael Boylan-Kolchin 343

The Circumgalactic Medium
Jason Tumlinson, Molly S. Peeples, and Jessica K. Werk 389

How to Characterize Habitable Worlds and Signs of Life
Lisa Kaltenegger 433

Indexes

Cumulative Index of Contributing Authors, Volumes 44–55 487

Cumulative Index of Article Titles, Volumes 44–55 490

Errata

An online log of corrections to *Annual Review of Astronomy and Astrophysics* articles may be found at http://www.annualreviews.org/errata/astro